Dynamic interactions of retroviral Gag condensates with nascent viral RNA at transcriptional burst sites: implications for genomic RNA packaging

Rebecca J. Kaddis Maldonado[1,2*] and Leslie J. Parent[1,2*]

Departments of [1]Medicine and [2]Microbiology & Immunology,

Penn State College of Medicine

500 University Drive

Hershey, PA 17033

*Co-corresponding authors

Email: rjk297@psu.edu and lparent@psu.edu

Abstract

Retroviruses are responsible for significant pathology in humans and animals, including the acquired immunodeficiency syndrome and a wide range of malignancies. A crucial yet poorly understood step in the replication cycle is the recognition and selection of unspliced viral RNA (USvRNA) by the retroviral Gag protein, which binds to the psi (Ψ) packaging sequence in the 5' leader, to package it as genomic RNA (gRNA) into nascent virions. It was previously thought that Gag initially bound gRNA in the cytoplasm. However, previous studies demonstrated that the Rous sarcoma virus (RSV) Gag protein traffics transiently through the nucleus, which is necessary for efficient gRNA packaging. These data formed a strong premise for the hypothesis that Gag selects nascent gRNA at transcription sites in the nucleus, the location of the highest concentration of USvRNA molecules in the cell. In support of this model, previous studies using fixed cells infected with RSV revealed that Gag co-localizes with large USvRNA nuclear foci representing viral transcriptional burst sites. To test this idea, we used single molecule labeling and imaging techniques to visualize fluorescently-tagged, actively transcribing viral genomes, and Gag proteins in living cells. Gag condensates were observed in the nucleus, transiently co-localized with USvRNA at transcriptional burst sites, forming co-localized viral ribonucleoprotein complexes (vRNPs). These results support a novel paradigm for retroviral assembly in which Gag traffics to transcriptional burst sites and interacts through a dynamic kissing interaction to capture nascent gRNA for incorporation into virions.

Keywords: retrovirus Gag proteins, genomic RNA packaging, retrovirus assembly, live cell imaging, transcriptional bursts, biomolecular condensates, Rous sarcoma virus

Introduction:

RNA synthesis is coordinated with critical steps in RNA processing, including 5' capping, splicing, polyadenylation, and 3' cleavage, all of which occur co-transcriptionally [1-8]. Many nuclear factors involved in these processes, including RNA polymerase II (RNAPII), transcription factors, and splicing machinery, coalesce into distinct nuclear foci that form dynamic biomolecular condensates (BMCs), also known as transcriptional condensates [9-13]. The co-transcriptional binding of these factors promotes efficient synthesis of fully-processed RNAs. The fates of cellular mRNAs are determined by specialized RNA binding proteins (RBPs) that bind during or shortly after mRNA synthesis [14-20]. Spliced mRNAs are licensed for export co-transcriptionally when members of the TREX complex and Nxf1 (Tap) are recruited during splicing [15]. Unspliced RNAs, in contrast, are typically retained in the nucleus to prevent the translation of aberrant proteins. In some cases, binding of nuclear export factors transport the mRNA to a specific subcellular location or organelle where it undergoes translation [21]. These complex co-transcriptional processes are essential and tightly regulated, yet the mechanisms governing them are incompletely understood.

The mechanisms governing mRNA fate are particularly relevant for retroviruses, which cause severe immunodeficiency syndromes and cancers in humans and a wide range of animal species. Retroviruses integrate their reverse-transcribed DNA into the host cell chromosome, behaving like cellular genes transcribed by RNAPII and decorated with a 5' cap and 3' polyadenylated tail. Nascent retroviral RNA (vRNA) can be spliced and exported by the usual route for processed genes. Alternatively, the vRNA can remain unspliced and must overcome the barrier for unprocessed RNAs to be exported from the nucleus into the cytoplasm, where the full-length vRNA serves as (i) mRNA for synthesis of the viral structural proteins Gag and GagPol, or (ii) genomic RNA (gRNA), which is captured by Gag for packaging into new virions that propagate infection [reviewed in [22]].

The mechanism by which unspliced retroviral RNAs (USvRNAs) are sorted into mRNA or gRNA at the transcription site is incompletely understood, despite the absolute requirement for each full length vRNA to produce infectious virus particles. Recently, a novel mechanism for

identifying the unspliced vRNA that serves as gRNA was proposed after finding that the retroviral Gag proteins of Rous sarcoma virus (RSV), human immunodeficiency virus type 1 (HIV-1), prototype foamy virus, murine leukemia virus, feline immunodeficiency virus, and Mason-Pfizer monkey localize to the nucleus [23-39]. In addition, both RSV and HIV-1 Gag undergo liquid-liquid phase separation to form biomolecular condensates (BMCs) [23,40-42], producing a high local protein concentration in distinct foci that permit the viral condensate to remain intact while travelling through the densely-packed intracellular environment to reach the plasma membrane for budding.

To gain further mechanistic insights into the potential role of Gag nuclear trafficking in gRNA packaging, the avian retrovirus RSV was used as an experimental system because its mechanisms governing nuclear import and export are the best understood among retroviral Gag proteins. For RSV, nucleocytoplasmic trafficking of Gag is required for efficient gRNA packaging [24,28-30]. In RSV-infected cells, large, bright foci of USvRNA can be visualized in the perichromatin space using single-molecule RNA FISH (smFISH) [24], representing transcriptional bursts of viral RNA synthesis arising at the chromosomal site of proviral integration [24]. In previous studies, we found that RSV Gag localizes preferentially to the euchromatin fraction of the nucleus and co-localizes with USvRNA at transcription sites, forming viral ribonucleoprotein complexes (vRNPs) that are seen crossing the nuclear envelope during nuclear egress [24].

In the present study, live cell, time-resolved confocal imaging experiments were performed to examine the spatiotemporal interplay of Gag condensates with USvRNA at viral transcription sites to better understand the nature of the interaction. These experiments revealed the surprising finding that condensates of Gag engaged in a transient kissing interaction with nascent retroviral RNA at transcriptional burst sites, reminiscent of the interaction of RNAPII, the transcription co-factor Mediator (Med19), and actively transcribing *Sox2* mRNA, resulting in enhanced expression of the target gene [11,13]. This type of kissing interaction between a viral protein and its cognate vRNA has not been described previously, therefore we sought to investigate its mechanism in more detail and examine whether the transient interaction of Gag with USvRNA at transcriptional burst sites plays a role in viral transcription regulation or gRNA packaging.

Results:

Dynamic interaction of RSV Gag with USvRNA at transcriptional bursts

Advanced imaging approaches and single molecule labeling has revealed that large amounts of RNA are synthesized during transcription to form transcriptional bursts [37,43]. In imaging studies, transcriptional bursts appear as large, very bright nuclear RNA foci, which we previously observed in RSV-infected cells using smFISH [24]. Up to now, Gag localization at viral transcription sites had only been observed in fixed cells, not allowing the movement of the protein and vRNA involved in the interaction to be examined on a dynamic time scale. We were interested in examining how rapidly Gag traffics to the vRNA burst and whether the interaction is stable or transient. To gain insight into these questions, the kinetics of Gag-USvRNA interactions in the nucleus of living cells were studied in a quail fibroblast cell line, QT6 rtTA TRE RC.V8 MS2 stbl, which constitutively expresses reverse tetracycline-controlled transactivator (rtTA), a modified RSV proviral construct controlled by a doxycycline-inducible promoter (TRE) and incorporates 24 copies of MS2 stable stem-loops between the *nucleocapsid* (*nc)* and *protease* (*pr)* coding regions to specifically label USvRNA [44] (Figure 1A). These cells were co-transfected with pNES1-YFP-MS2-NLS, which labels USvRNA by binding to the MS2 stem-loops co-transcriptionally. The brightest USvRNA object(s) in each nucleus were considered to be transcriptional bursts, consistent with previous reports [11,13]. A Gag-SNAPTag fusion protein was expressed to permit single-molecule detection of Gag. After doxycycline treatment, cells were incubated with the SNAPTag ligand JF549 and imaged at ~1

frame/sec for approximately 6 minutes using confocal microscopy. Discrete condensates of Gag (red) and a large USvRNA focus (green) representing the transcriptional burst site were observed. To our surprise, these foci exhibited dynamic movement, forming kissing interactions, with Gag and vRNA foci coming together and co-localizing, then moving apart multiple times over the imaging period (Figure 1B and Supplementary Movie 1). A kissing interaction was defined as co-localization of Gag and USvRNA foci at a distance of ≤0.250 μm, based on the resolution limit of the microscope objective in the x-y plane.

To assess the temporospatial dynamics, particle tracking was performed to measure how rapidly co-localization and separation between the Gag condensate and vRNA burst occurred over time. Images corresponding to individual timepoints are displayed in Figure 1B, with the tracks shown in Figure 1C corresponding to the timelapse images in Supplementary Movie 1. The distances between Gag and USvRNA changed rapidly over time, with instances of separation (>0.25 μm) followed by close proximity (≤0.250 μm) in as little as 5s (Figure 1B, timespans 0-4.2 s and 13-18 s). The cycles of to-and-fro movement between the Gag condensate and USvRNA burst varied in duration, with the foci remaining in close proximity for ~ 34 s (53-91.5 s), followed by separation (>0.250 μm) for 85 s (timepoints 92.6-182 s), before coming back together (183-215 s) for 30 s. In contrast, the co-localization of Med19 condensates with the *Sox2* mRNA active gene locus lasts longer, on the order of 5-10 minutes [13]. These data suggest that the mechanism that controls the Gag-USvRNA interaction differs from the regulation of kissing between the *Sox2* mRNA and transcriptional condensates. It is possible that the mechanisms of contact serve different purposes, for example the shorter “hit-and-run” between Gag and USvRNA could mediate gRNA packaging, whereas the longer contact is needed for transcriptional condensate-mediated gene expression [45].

Measurements of the distances between the Gag condensate and UsvRNA burst indicated that they were ≤1 μm apart at all timepoints (Supplementary Movie 1), suggesting an active mechanism maintains their close proximity. Quantitation of the fluorescence intensity of the Gag condensate demonstrated that it increased over time (Figure 1D). Simultaneously, the USvRNA fluorescence intensity decreased (Figure 1D) and eventually disappeared (300 s timepoint), possibly due to a decrease in transcriptional activity, transfer of RNA molecules from the burst to a Gag condensate, movement of the RNA outside the plane of imaging, or bleaching of the fluorophores labeling the USvRNA. Although the intensity of the Gag focus increased, the condensate area remained unchanged (ranging from 0.1-0.22 μm^2), suggesting that the intensity increase was not caused by a change in the size of the condensate but due to an increase in the number of Gag molecules densely packing into the condensate (Figure 1E). Furthermore, there was an inverse correlation between the intensities of the Gag condensate and the USvRNA burst (Pearson’s correlation (r) = -0.693, p<0.0001) (Figure 1D). One possible explanation for this anti-correlation is that Gag molecules accumulate in the condensate, bind to USvRNA to form a vRNP complex, which moves away from the burst, resulting in a decrease in Gag intensity. At that point, bursting of viral transcription occurs again, with an increase in fluorescence intensity of the USvRNA focus, and the cycle repeats. The complexity of the relationship between transcriptional bursting and protein condensates has been described for cellular factors yet remains poorly understood [9,11,13]. Technical advances in super-resolution imaging or other biophysical techniques will be needed to dissect how and why newly transcribed USvRNA and Gag engage in such complex choreography.

Quantitative analysis of a second live cell experiment demonstrated numerous to-and-fro movements between a Gag condensate and an USvRNA transcriptional burst site (1 of 3 bursts) (Figure 2A-C; Supplementary Movie 2). This cell contained three bursts, due to Piggybac integrating into multiple sites. Only one burst was tracked in this movie. Particle tracking of the Gag condensate and USvRNA burst site indicated that they remained within close proximity (0.7 μm) of one another during the 3 minute duration of imaging (Figure 2B). The Gag condensate moved towards the transcriptional burst and underwent co-localization in ~51

s. The kissing interaction was initially brief, and the distance between the Gag condensate and USvRNA then fluctuated from near to far between timepoints 56-102 s. Following that initial contact, there was a long period of co-localization lasting 28 s (timepoints 101.8-129.2 s) followed by a long separation (43 s; timepoints 129.2-172.2 s) and then a brief period of co-localization. Similar to the data shown in Figure 1D, the fluorescence intensity of the Gag condensate signal was anti-correlated with the USvRNA intensity ($r = -0.454$, $p<0.0001$, analyzed from 1-200s, Figure 2C).

At a different time point in the same cell, we observed multiple Gag condensates near two separate transcriptional bursts (Figure 2D, Supplementary Movie 3). This set of images indicated that more than one Gag condensate can enter the nucleus and make transient contact with more than one USvRNA burst sites. Two of those Gag condensates were tracked and even though there were two USvRNA bursts, the Gag condensates appeared to favor the burst on the left over the burst on the right. We have observed this phenomenon previously in acutely infected fixed cells where Gag was co-localized with one burst but not the other [24]. It is feasible that the bursts are at different stages of transcription and Gag preferentially co-localizes with one stage over the other. Another possibility is that the nuclear topology blocks access of the Gag condensate to one of the vRNA transcription sites due to its location on a particular euchromatin loop or the local environment of the proviral integration site. Further studies will be needed to investigate these possibilities.

Live cell particle tracking (Figure 2D and E; Supplementary Movie 3) revealed that condensate #1 (labeled as Gag 1 with the yellow arrow and track) appeared at the burst earlier in the imaging period compared to condensate #2 (Gag 2, white arrow and track). Gag condensate #1 was co-localized with the USvRNA burst for ~40s, and as it moved away from the vRNA, Gag condensate #2 moved toward the USvRNA burst and became co-localized. Consistent with Figures 1D and 2C, the intensities for Gag condensates #1 and #2 were inversely correlated to the intensity of the USvRNA transcriptional burst throughout the course of the real time imaging period shown in Figure 2F (Gag 1 intensity to USvRNA intensity: $r = -0.180$, $p=0.024$; Gag 2 intensity to USvRNA intensity: $r = -0.363$, $p=0.001$).

To determine whether Gag-USvRNA kissing interactions could be observed at shorter periods after doxycycline induction, cells were induced for only two hours before imaging (Figure 3A, Supplementary Movie 4). A Gag focus initially visualized in the cytoplasm (white arrowhead, Figure 3A; 0 s) subsequently crossed into the nucleus (dashed white line), moving toward the burst of USvRNA transcription. The elapsed time from when the Gag condensate entered the nucleus and trafficked to the transcription site was rapid (~173 sec). Once the Gag condensate entered the nucleus, it took ~137 s to co-localize (≤0.25 μm) with the USvRNA burst, and displayed a “hit-and-run” interaction with the burst over a period of 30 sec (309.8 s-339.2 s). The USvRNA burst was positioned near the nuclear rim, as reported for actively transcribing genes [46], near the point where Gag entered the nucleus, which could explain how the Gag condensate trafficked to the transcriptional burst with rapid kinetics.

From the time the Gag condensate entered the nucleus, it remained in close proximity with the USvRNA burst (≤0.9 μm; Figure 3B) for over 5 minutes, until the end of the imaging time. The intensity of the Gag signal remained constant from its position in the cytoplasm throughout its stay in the nucleus (Figure 3C). However, the RNA signal diminished over time, possibly due to a decrease in transcriptional activity, movement out of the imaging plane, or bleaching of the fluorescence signal from imaging (Figure 3C). The intensities of the Gag and USvRNA signals were inversely correlated, as seen in each of the previous episodes ($r = -0.329$, $p<0.0001$).

We previously reported that Gag interacts with the nuclear export protein CRM1 to mediate its nuclear egress [29,47], therefore we sought to observe Gag-USvRNA complexes leaving the nucleus. In the still images extracted from Supplementary Movie 5 (shown in Figure 4A), a Gag condensate co-localized with an USvRNA focus in the nucleus and the vRNP

complex trafficked toward the nuclear rim (372 s) into the cytoplasm. This USvRNA focus was not defined as a transcriptional burst site because other USvRNA foci were brighter in the cell. A co-localization channel was created to better visualize the vRNP complex (Figure 4A inset, upper right corner, white signal and track; see also Supplementary Movie 6), which moved to the nuclear rim and into the cytoplasm. The co-localized condensate moved in a to-and-fro fashion along the nuclear edge several times during the movie, and once in the cytoplasm always remained co-localized (≤0.25 µm) (Figure 4B).

The Gag condensate intensity changed in an undulating pattern over time (Figure 4C), suggesting that additional Gag molecules were joining and leaving the condensate, or alternatively, the signal was moving in and out of the imaging plane. In contrast to the previous Gag condensates that transiently kissed the USvRNA bursts, the Gag and USvRNA signals remained co-localized and the intensities were positively correlated ($r=0.250$, $p<0.0001$). The observation that this Gag-USvRNA complex moved out of the nucleus and into the cytoplasm, suggests that this vRNP represents an early step in gRNA packaging.

RSV Gag condensates co-localized with nascent USvRNA at viral transcription sites

To rigorously test whether RSV Gag was binding to nascent USvRNA at the viral transcription site, QT6 rtTA TRE RC.V8 Gag-SNAPTag MS2 stbl cells (Figure 5A) were dox-induced for 48 hours and incubated with 5-Ethynyl Uridine (EU). In this cell line, the SNAPTag was inserted in frame at the C terminus of Gag. Nascent RNA was pulse-labeled with EU for 10 minutes to label viral and cellular RNA, which was detected using click chemistry, and smFISH was used to specifically detect USvRNA. Cells were fixed, imaged with confocal microscopy, and three-dimensional cross-sections were generated from Z-stacks (Figure 5B). Three-way signal-based co-localization (yellow) analysis revealed that the USvRNA (green), Gag-SNAPTag (red), and EU (gray) were co-localized in the nucleus (dashed white line). Figure 5C shows an enlargement of the area of interest to illustrate the 3-way co-localization, indicating that nuclear Gag was associated with newly transcribed USvRNA at active transcription sites.

RSV USvRNA transcriptional bursts were located within 1 µm of nuclear edge

Given that the HIV-1 provirus preferentially integrates within 1 µm of the nuclear envelope [35,48], we performed confocal imaging experiments to determine the location of RSV transcriptional bursts and Gag condensates in infected cells. Chronically infected cells were subjected to simultaneous immunofluorescence/ smFISH to label Gag and USvRNA, respectively. Although the proviral DNA was not directly labeled, the provirus serves as the template for viral RNA synthesis and therefore, the USvRNA transcriptional burst site was at the same location as the integrated provirus. Each of the USvRNA bursts was <1.0 µm (mean = 0.31 µm ± 0.03 µm) from the edge of the nucleus (defined by DAPI) in three dimensions, indicating that like HIV-1, RSV integrates close to the nuclear rim (Figure 6A, Supplementary Table 1). Similarly, nearly all of the Gag condensates (91.8%) in the nucleus were located within 1 µm of the nuclear periphery (mean distance = 0.14 µm ± 6.81×10^{-3} µm; Figure 6B, Supplemental Table 2). Together, these data indicate that both Gag and the USvRNA bursts were positioned near the edge of the nucleus, therefore Gag condensates do not need to travel far into the nucleoplasm in search of the USvRNA burst. It is not clear whether nuclear Gag molecules located farther inside the nucleus could be performing other functions, such as altering chromatin organization, splicing, or other cellular processes [49].

Complex morphology of USvRNA transcriptional bursts revealed by STED microscopy

The high intensity of transcriptional bursts is attributed to the large quantity of nascent RNA being produced, with individual RNA molecules undergoing different stages of transcription, and co-transcriptional RNA processing steps [11,13,50,51]. To elucidate more structural detail of the RSV USvRNA bursts in infected cells, we used super-resolution STED microscopy

(green) and compared that method to images obtained by confocal microscopy (red). smFISH probes complementary to the RSV intronic sequence were used to specifically detect USvRNA, and the inner leaflet of the nuclear membrane was outlined with Sun1-Venus (blue)(Figure 7).

In a single z-slice (Figure 7A), the signals from the confocal and STED images overlapped, as expected, but there was more detail seen in the STED images (Figure 7A). A three-dimensional reconstruction was generated with orthogonal clipping planes of surface renderings of the transcriptional burst showing that the contour of the RNA signal looked smooth and indistinct in the confocal images, whereas using STED, the burst surfaces appeared sharper, with multiple connected nodes visualized (Figure 7B). These nodes could indicate regions of high level of transcriptional activity during bursting as additional molecules of RNAPII are recruited to the integrated proviral DNA [51]. To show more detail, magnified images of two different bursts are shown in panels C and D. In both cases, multiple foci of RNA appeared to be connected, forming a complex structure, which may represent RNA emanating from clustered transcriptional condensates [52,53]. Surface rendering of the bursts in C and D (insets) allowed the three-dimensional structure to be appreciated, demonstrating the complex architecture of the RNA signal. Although these two bursts contained multiple foci, other burst sites had more condensed USvRNA and appeared as single foci (data not shown), which is to be expected, given the stochastic nature of transcriptional bursting [11,13,52]. This cell-to-cell heterogeneity suggests that RSV transcription sites are at different stages of the bursting cycle in each cell (and even within a single cell containing two integration sites), and the larger bursts are likely more active compared to the compact foci.

Gag proximity to the transcriptional burst site did not enhance viral gene expression

The live cell imaging experiments shown in Figures 1-3 and the Supplementary Movies required that the USvRNA and Gag protein were altered by the insertion of exogenous tags to detect fluorescence signals. However, because such tags can affect RNA and protein trafficking, we performed quantitative analysis of images obtained using simultaneous immunofluorescence and smFISH in RSV-infected cells. Confocal z-stacks of cells were deconvolved and surfaces were generated using Imaris analysis software. The brightest USvRNA object(s) in each nucleus were considered to be transcriptional bursts, consistent with previous reports [11,13].

We observed Gag at transcriptional burst sites in the nucleus of infected cells (Figure 8A) and found that most (51%) of the nuclear Gag condensates located nearest to an USvRNA burst were within 1 µm (Figure 8B). In some cases, multiple Gag condensates were located a similar distance from the same transcriptional burst site (Figure 2D; Supplementary Movie 3). Using the Imaris surface function, we compared the intensities of Gag condensates close to USvRNA bursts to the intensities of Gag foci farther away from the bursts. The Gag condensates closest to the bursts (mean intensity 299.4 A.U. ± 34.96) were significantly brighter than those farthest from the bursts (198.9 A.U. ± 6.14 A.U.; $p<0.0001$) (Figure 9C). Interestingly, although the intensities of Gag foci closest to the burst were higher, there was no significant difference in the volumes of the foci, suggesting that the Gag condensates remained the same size regardless of their position (Figure 8D). Similarly, this finding is consistent with the observations from the live cell imaging experiments in which additional Gag molecules were recruited to the condensates over time, resulting in an increase in fluorescence intensity.

In previously described cases of kissing between mRNA and transcriptional condensates, the close distance (<1 µm) between transcriptional condensates and the gene locus was associated with an increase in gene expression [11,13,54]. Because we found that Gag condensates were close to USvRNA transcriptional burst sites (mean distance of 0.54 µm), we examined whether Gag altered viral transcriptional activity. Quantitative analysis revealed very low correlation between Gag proximity to the USvRNA burst and the volume (Figure 8E; $r = -0.13$) or intensity (Figure 8F; $r =0.02$) of the RNA focus, suggesting that Gag did not affect the

level of USvRNA synthesis under these experimental conditions. These data indicate that the mechanism by which Gag is recruited to the USvRNA burst may not involve Gag interaction with an active transcriptional condensate. Gag may instead interact with a different host factor(s) for targeting to the active viral transcription site. These candidates may include members of the Mediator complex, transcription factors, splicing factors, and chromatin remodelers that we identified as potential Gag-interacting partners in a previous proteomic study [49]. Further studies will be needed to assess whether Gag alters the activity of cellular genes, which was not tested in these experiments.

Taken together, the data presented herein indicate that RSV Gag condensates enter the nucleus and interact with USvRNA burst sites co-transcriptionally through a dynamic kissing mechanism, in a similar fashion as transcriptional condensates with cellular genes [11,13]. Furthermore, we presented evidence that the Gag-USvRNA complexes formed at sites of vRNA synthesis are subsequently exported from the nucleus, possibly for the purpose of encapsidation of gRNA into nascent virions.

Discussion:

Retroviruses cause severe disease including cancer and lethal immunodeficiencies, yet significant portions of the replication cycle remain poorly understood. Despite the absolute requirement for encapsidation of the viral genome for infectivity, it remains uncertain how retroviral Gag proteins find their RNA genomes for assembly into virions. Previously, it was shown that RSV Gag nuclear trafficking is required for efficient gRNA packaging, raising the possibility that recognition and capturing of gRNA occurs in the nucleus [24,30]. The Gag proteins of RSV and HIV-1 oligomerize to form BMCs, localize to viral transcription sites in the nucleus, and may interact with host transcription machinery, chromatin modulators, and splicing factors [24,25,35,37,40-42,49]. Many key questions remain unanswered regarding how Gag condensates interact with cellular machinery to traffic to viral transcription sites, recognize and bind gRNA, and form vRNP complexes to nucleate assembly of virus particles [23-25,35,37,49].

In the present study, we use live cell confocal microscopy and quantitative imaging analysis to gain insight into the mechanism by which the RSV Gag protein interacts with active viral RNA transcription sites. To our knowledge, the present study is the first to demonstrate a dynamic interaction of viral condensates with nucleic acids; in contrast, previous examples of kissing condensates involved cellular transcription clusters, enhancers, and mRNA synthesized at transcriptional bursts [11,13].

In our live-cell experiments, we observed Gag condensates transiently co-localizing with nascent USvRNA at transcriptional burst sites, presumably where the proviral DNA was integrated into the host chromosome. Kissing was defined as co-localization (distance of ≤0.25 µm) of Gag condensates with the USvRNA (Supplementary Movies 1-4, Figures 1-3). We were able to capture a Gag condensate enter the nucleus via the nuclear pore closest to the transcription site before kissing the burst (Supplementary Movie 4, Figure 3), suggesting that this phenomenon is directed. Gag appeared to enter the nucleus within close proximity of the USvRNA raising the possibility that perhaps Gag selectively enters through specific nuclear pores [55,56]. Additional studies are needed to test that idea.

Our previous studies revealed that HIV-1 Gag localizes within 1 µm of the edge of the nucleus and preferentially co-localizes with transcriptionally-active euchromatin marks [35], suggesting that HIV-1 Gag interacts with euchromatin-bound factors to find sites of USvRNA synthesis. RSV Gag and USvRNA bursts also localized within 1 µm of the nuclear rim (Figure 6B), it is possible that RSV Gag utilizes a similar mechanism to target active viral transcription sites.

Using confocal microscopy, transcriptional bursts appeared as large bright foci, however, STED revealed that many bursts contained multiple small foci in clusters that could correlate to

single RNAs (Figure 7) at different stages of RNA synthesis, similar to super-resolution images of RNA polymerase II clusters [52]. The dynamics of RNA bursting has been reported to be regulated by the proximity of transcription factors to the promoter, the number of transcription factor binding sites present, and the binding affinity [50]. It is hypothesized that transcription factors, such as members of the Mediator complex, bind to clusters of enhancers, and use the dynamic movement between the enhancer and promoter to interact with transcriptional condensates in a transient kissing interaction that involves CTCF and cohesin [11]. These data suggest that the mechanism by which the kissing occurs involves the looping out of the chromatin by the cohesin and CTCF to bring transcriptional condensates into close proximity of the *Sox2* gene locus. In the case of the kissing between RSV Gag and the USvRNA burst, although the Gag does not change the bursting dynamics of the USvRNA, it is possible that chromatin looping is involved in the movement of Gag condensates toward the active viral transcription sites and this hypothesis will be important to investigate. Because kissing interactions in the nucleus can occur within or between chromosomes to regulate gene expression [57,58], it is possible that Gag takes advantage of these chromatin rearrangements to come into close proximity of the USvRNA burst. Furthermore, the RSV Gag interactome includes Mediator family members, RNAPII subunits, and splicing factors [37,49], that may be responsible for the interaction of RSV Gag with USvRNA-containing transcriptional condensates.

In our proposed model (Figure 9), Gag traffics into the nucleus and initially forms a condensate that is distinct from transcriptionally-active condensates. RSV Gag has been observed to interact with splicing factors and to traffic through nucleoli where snRNPs involved in splicing are generated [26,37,49]. Because nucleoli and splicing speckles are BMCs and produce factors that are required for RNA synthesis and processing, it is possible that Gag forms co-condensates and interacts with factors that traffic to the transcription site [23,59]. We hypothesize that when the Gag condensate kisses the USvRNA transcription site, it binds to USvRNA and selects it for packaging. This hypothesis is compelling because co-transcriptional selection of gRNA by Gag would increase packaging efficiency. Gag binding to the psi (Ψ) packaging sequence in the USvRNA causes a conformational change in Gag that exposes the nuclear export signal, and allows it to bind CRM1 to mediate Gag egress through the nuclear pore complex [29]. This Gag-USvRNA complex then becomes the starting material for assembly of new virions at the plasma membrane.

Methods:

Plasmids and cell lines:

Experiments were performed using chemically transformed QT6 quail fibroblast cells which were maintained and transfected via the calcium phosphate method as previously described [60-62].

Many of the constructs used to create the TRE RC.V8 constructs with internal tagged Gags and MS2 stemloops were based upon the cloning strategy used to clone pRC.V8 Gag-CFP 24xMS2 constructs, which was previously described [24]. To create PB TRE RC.V8 MS2 stbl, first the region of RC.V8 encoding from the PmlI restriction site in *pol* to the end of the 3'LTR was amplified using primers 5'-TCTCCACGTGCGGAGTCATTCTGA-3' and 5'-CGATGCGGCCGCCCCTCCGACGGTACTCAGCTTCTG-3', and inserted into the PmlI and NotI sites of a piggybac TRE RC.V8 RU5 Gag.Pol mCherry construct with the first two ATG codons mutated to ATA to prevent translation (unpublished data) (PB TRE RC.V8 2ATG-ATA). To correct the ATA mutations to functional ATGs, PB TRE RC.V8 2ATG-ATA was digested with PmlI and NotI, and swapped with the corresponding sites in a PB TRE Gag-Pol plasmid containing functional ATGs to create PB TRE RC.V8. To insert 24 copies of MS2 stemloops, a restriction fragment from an RC.V8 derived construct that contained a stop codon after *nc* with

24 copies of MS2 stable stemloops between *nc* and *pr* were cloned into the FseI and PmlI sites of PB TRE RC.V8 to create the final PB TRE RC.V8 MS2 stbl construct. The location of the MS2 RNA stemloops between *nc* and *pr* allows for the specific labeling of unspliced viral RNA only by the MS2 coat protein. pCR4-24XMS2SL-stable was a gift from Robert Singer (Addgene plasmid # 31865; http://n2t.net/addgene:31865 ; RRID:Addgene_31865).

To create the PB TRE RC.V8 Gag-SNAPTag MS2 stbl construct, an RC.V8 derived construct that contained *gag-SNAPTag* and 24 copies of MS2 stemloops between *SNAPTag* and *pr* were cloned into the FseI and PmlI sites of PB TRE RC.V8 to create the final PB TRE RC.V8 Gag-SNAPTag MS2 stbl construct.

pSun1-Venus was created using Gibson assembly [63], with fragment 1 obtained by digesting pVenus-N2 with NheI and BamHI. The sequence encoding *sun1* (fragment 2) was amplified from pDEST-Sun1-mCherry (a gift from Jan Karlseder, Salk Institute for Biological Studies [64]) using primers 5'-ACCGTCAGATCCGCTAGCGCTATGGATTTTTCTCGGCTTCACATGTACAGT-3' and 5'-CTCGCCCTTGCTCACGGATCCGGTGGCGACCGGTCCGATCA-3' and was flanked by sequences that overlap the ends of fragment 1. pMS2-Halo-NLS was cloned by PCR amplifying the *halo* tag region from PB-H2B-Halo using primers 5'-ATCGACCGGTCGCCACCGGGATCCACGAAATCGGTACTGGCTTTCCATTCGACCCCCATT-3' and 5'-CGATATCGATTTATACCTTTCTCTTCTTTTTTGGGGAAATCTCCAGAGTAGACAGCCAGC -3', and inserted into the AgeI and ClaI restriction sites in pMS2-YFP-NLS [44,65,66]. LZ10 PBREBAC-H2BHalo was a gift from James Zhe Liu (Addgene plasmid # 91564; http://n2t.net/addgene:91564; RRID:Addgene_91564) [67]. The pGag-SNAPTag, NES1-YFP-MS2-NLS, and PB-t-rtTA were previously described [23-25].

To create the QT6 rtTA PB TRE RC.V8 MS2 stbl cell line, QT6 cells were seeded in a 35 mm dish at $0.3x10^6$ and transfected the next day with 3 µg of PB TRE RC.V8 MS2 stbl and 1.2 µg of transposase (System Biosciences) for a ratio of 0.2 µg of transposase per 500 ng of piggybac vector using the calcium phosphate method [24]. Two days later the cells were transferred to a 100 mm dish. When the cells were ~95% confluent, they underwent puromycin selection with 3 µg/mL of drug. Following testing and selection of the cell line, 1 µg of pPB-t-rtTA and 0.4 µg of transposase was transfected into the PB TRE RC.V8 MS2 stbl cell line. The QT6 rtTA PB TRE RC.V8 MS2 stbl cell line was subjected to selection with 2 µg/ml blasticidin. The QT6 rtTA PB TRE RC.V8 Gag-SNAPTag MS2 stbl cell line was created in the same fashion except the PB TRE RC.V8 Gag-SNAPTag MS2 stbl construct was transfected along with transposase using the same DNA amounts as before in a QT6 cell line that already expressed rtTA (QT6 rtTA). Piggybac transfections lead to multiple integration sites, which accounts for multiple bursts.

RC.V8 infection of QT6 cells:

To create RC.V8-infected cells, uninfected QT6 cells were seeded into a 100 mm dish and the next day transfected with 10 µg of pRC.V8 via the calcium phosphate method. The next day, the media was changed. Virions were collected for ~48 hours, centrifuged for 5 minutes at 2000 rpm at room temperature to remove dead cells, and added to naïve QT6 cells. Cells were infected at 37°C for 4 hours before changing the media. Cells were carried for prolonged periods.

Simultaneous Immunofluorescence/smFISH:

To visualize USvRNA and *cis*-expressed Gag in infected cells, cells were seeded at 0.5 x 10^6 onto #1.5 coverslips. If cells were to be used for STED microscopy, they were transfected with 25 ng of pSun1-Venus via calcium phosphate to delineate the inner leaflet of the nuclear membrane for 16 hours. Cells were quick rinsed with RNase-free 1x PBS and fixed for 10

minutes in RNase-free 3.7% formaldehyde at room temperature, followed by 2x 5 minute washes with 1x PBS. The fixed cells were dehydrated in 70% ethanol at 4°C for a minimum of 24 hours. Cells were rehydrated in wash buffer (WB: 10% formamide, 2x SSPE, DEPC H_2O) for 20 minutes at room temperature. Coverslips were incubated in a humid chamber for 16- 20 hours at 37°C with 100 µl of hybridization buffer (10% dextran sulfate, 2x SSPE, 10% formamide) containing 1 µl of a 25 µM stock of 42 Stellaris RNA smFISH probes conjugated to Quasar 570 tiling the *gag* coding region (Biosearch) and mouse anti-RSV capsid primary antibody (made by Dr. Neil Christensen, Penn State College of Medicine) at 1:100. The next day, coverslips were incubated for 30 minutes at 37°C in WB containing donkey anti-mouse Alexa 647 (Thermo Fisher Scientific) at 1:1000. Coverslips were washed once more in WB for 30 minutes at 37°C either with (confocal) or without (STED) DAPI, and mounted in ProLong Diamond (Thermo Fisher Scientific).

EU labeling of nascent RNAs:

To visualize nascent RNAs, cells were pulse labeled with EU and labeled with Alexa 488 using the Molecular probes Click-IT RNA imaging kit. To visualize nascent RNAs in the QT6 rtTA TRE RC.V8 Gag-SNAPTag cell line, cells were seeded on coverslips as above and dox-induced for 48 hours. In the last hour, Gag-SNAPTag was labeled with 100 nM JF646 SNAP ligand [a kind gift from Luke Lavis, Janelia Research Campus [68]]. In the last 10 minutes, cells were pulse labeled with 1mM 5-ethynyl uridine (EU) at 37°C. Next, cells were rinsed 2x with 1x PBS, fixed for smFISH as above, and incubated overnight at 4°C in 70% ethanol. Following 20 minutes of rehydration in WB, cells were rinsed 1x in 1x PBS and subjected to the Click-IT (click-chemistry) reaction to label the RNA with Alexa 488 for 30 minutes at room temperature. Coverslips were washed 1x in Click-IT rinse buffer and 1x in 1x PBS. The FISH protocol was then completed as outlined above (without antibodies).

Confocal Microscopy:

For IF/FISH imaging, slides prepared as outlined above were imaged on a Leica AOBS SP8 FALCON confocal microscope equipped with hybrid detectors with time gating and a white light laser. Single fluorophore and secondary antibody controls were imaged to confirm that there was not any background or crosstalk. Slides were imaged with a 63x/NA 1.4 oil objective at a pixel format at 1024x1024, a scan speed of 400 Hz, and a 3x zoom. Z-stacks were captured at a step size of 0.3 µm with sequential scanning. Gag labeled via immunofluorescence was excited with a 647 nm laser line at 11% power and collected with a hybrid detector set to 652 nm-774 nm with a frame average of 2. USvRNA was excited with a 555 nm laser at 5% power and collected with a hybrid detector at 565 nm- 630 nm with a frame average of 2.

The EU and Gag labeled QT6 rtTA TRE RC.V8 Gag-SNAPTag cell lines that were dox-induced for 48 hours were imaged similarly to infected cells except Gag-SNAPTag JF646 was excited with a 647 nm laser at 15% and collected from 652 nm-777 nm with a frame average of 4. USvRNA was excited with the 555 nm laser at 5% power and collected from 560 nm- 630 nm with a frame average 4. EU Alexa 488-labeled RNA was excited with 488 nm laser at 5% power and collected from 493 nm- 540 nm with a frame average of 4. DAPI was excited with the 405 nm laser at 10% power and collected with a PMT with a frame average of 4

For live cell timelapse microscopy, QT6 rtTA TRE RC.V8 MS2 stbl cells were seeded onto glass bottom dishes (Mattek) at 0.5 x 10^6 cells/dish. The next day, cells were transfected with 1 µg pNES1-YFP-MS2-NLS, and 500 ng of pGag-SNAPTag into transfection medium (5% fetal bovine serum (FBS) in DMEM) containing 2 µg/mL doxycycline to induce RC.V8 expression from the Tetracycline response element promotor. One hour before imaging, cells were incubated with 50 nM of SNAPTag ligand JF549 [a kind gift from Luke Lavis, Janelia Research Campus [68]] for 1 hour at 37°C to label Gag-SNAPTag fusion proteins. Cells were

washed and imaged in imaging medium (clear DMEM with L-glutamine, 4.5 mg/liter D-glucose, 25 mM Hepes (Gibco) supplemented with 5% FBS, 9% tryptose phosphate broth and 1% chicken serum) at 16-22 hours post induction. Cells were imaged between lines on a Leica AOBS SP8 FALCON confocal microscope in a live-cell incubated stage at 37°C, 5% CO_2 with a 63x/NA 1.2 water immersion objective at a rate of 1000 Hz at a frame every ~1 second and a pixel size of 512 x 512. NES1-YFP-MS2-NLS was excited at 514 nm with 3% power and collected with a hybrid detector at 524 nm – 552 nm with time gating. Gag-SNAPTag JF549 was excited at 557 nm with 1% power and collected with a hybrid detector from 562 nm – 648 nm with time gating. Where applicable, NucSpot 650 live cell nuclear stain was excited with 653 nm at 3% laser power and collected with a PMT at 663 nm- 779 nm.

Stimulated emission depletion (STED) super-resolution microscopy

For STED imaging of fixed cells, cells were prepared as above, without DAPI staining but with 25 ng of pSun1-Veus transfected to label the nuclear rim. Cells were imaged between lines on a Leica AOBS SP8 confocal microscope equipped with a STED module using a 100x/NA 1.4 oil immersion objective at 1000 Hz and a pixel format of 2048 x 2048. USvRNA was excited at 561 nm at 5% power and collected with a hybrid detector from 571 nm- 620 nm, and depleted with the 775 nm laser at 50%. Sun1-Venus was excited with 514 nm at 6% laser power and collected with a hybrid detector from 524 nm- 551 nm and depleted with the 592 nm laser at 30%. The Sun1 channel was also imaged with a frame accumulation of 2. All channels were imaged with Z STED at 50%.

For comparison between confocal and STED images of the USvRNA channel, the confocal channel was excited with the 561 nm laser at 10% power and collected with a hydrid detector at 571 nm-620 nm with a line accumulation of 2. The STED channel was excited and collected the same way except with depletion with the 660 nm laser at 50% and Z STED at 40%. Sun1-venus was imaged under confocal conditions. It was excited with a 514 nm laser at 10% power and collected with a hybrid detector at 524 nm – 541 nm with a line accumulation of 2.

Quantitative image processing and data analysis:

All confocal images and some STED images were deconvolved using Huygens Essential (SVI) using the classical maximum likelihood estimation (CMLE) deconvolution algorithm. Deconvolved z-stacks were further processed (Gaussian filters and histogram adjustments) and analyzed using Imaris image analysis 10.1.1 (Bitplane). The Imaris built-in machine learning algorithm was used to create surfaces of the DAPI (confocal), USvRNA, Gag, and EU channels. Any Gag, USvRNA, and EU surfaces outside of the nucleus were filtered out and removed from the analysis. Surface statistics were obtained including volume (μm^3), sum signal intensity, distances between objects, and distance from the edge of the nucleus. The brightest RNA foci in each cell as determined by surface statistics were identified as transcriptional bursts [11,13].

Confocal and STED comparison images were deconvolved using the Huygens Essential low STED signal template. Surfaces of the Sun1 signal were created in Imaris using manual surface creation. Gag and RNA surfaces were created using machine-learning as above.

For live cell particle tracking, the Imaris spot function was used to identify Gag and USvRNA foci to determine the distance between Gag and the transcriptional burst over time. Also, the signal-based co-localization function in Imaris was used to generate a co-localization channel.

Graphs were generated and statistical analyses was performed in Prism (GraphPad) using an unpaired two-tailed *t* test. Outliers were identified and removed using a ROUT test, where appropriate. Pearson's correlation (r) was used to determine the intensity correlations

between Gag and USvRNA, and correlations between Gag distance to burst vs burst intensity/volume.

Four replicates (42 cells) were analyzed for IF/FISH confocal analysis. For STED imaging of transcriptional bursts, three replicates were conducted, and 18 and 14 cells were imaged for STED alone and STED versus confocal analyses, respectively.

References

1 Shine, M. *et al.* Co-transcriptional gene regulation in eukaryotes and prokaryotes. *Nat Rev Mol Cell Biol* **25**, 534-554 (2024). https://doi.org/10.1038/s41580-024-00706-2

2 Shenasa, H. & Bentley, D. L. Pre-mRNA splicing and its cotranscriptional connections. *Trends in genetics : TIG* **39**, 672-685 (2023). https://doi.org/10.1016/j.tig.2023.04.008

3 Osheim, Y. N., Miller, O. L. & Beyer, A. L. RNP particles at splice junction sequences on Drosophila chorion transcripts. *Cell* **43**, 143-151 (1985). https://doi.org/10.1016/0092-8674(85)90019-4

4 Perales, R. & Bentley, D. "Cotranscriptionality": the transcription elongation complex as a nexus for nuclear transactions. *Mol Cell* **36**, 178-191 (2009). https://doi.org/10.1016/j.molcel.2009.09.018

5 Li, Y., Wang, Q., Xu, Y. & Li, Z. Structures of co-transcriptional RNA capping enzymes on paused transcription complex. *Nat Commun* **15**, 4622 (2024). https://doi.org/10.1038/s41467-024-48963-1

6 Garg, G. *et al.* Structural insights into human co-transcriptional capping. *Mol Cell* **83**, 2464-2477.e2465 (2023). https://doi.org/10.1016/j.molcel.2023.06.002

7 Aitken, S., Alexander, R. D. & Beggs, J. D. Modelling reveals kinetic advantages of co-transcriptional splicing. *PLoS Comput Biol* **7**, e1002215 (2011). https://doi.org/10.1371/journal.pcbi.1002215

8 Kyburz, A., Friedlein, A., Langen, H. & Keller, W. Direct interactions between subunits of CPSF and the U2 snRNP contribute to the coupling of pre-mRNA 3' end processing and splicing. *Mol Cell* **23**, 195-205 (2006). https://doi.org/10.1016/j.molcel.2006.05.037

9 Pei, G., Lyons, H., Li, P. & Sabari, B. R. Transcription regulation by biomolecular condensates. *Nat Rev Mol Cell Biol* (2024). https://doi.org/10.1038/s41580-024-00789-x

10 Mir, M. *et al.* Dynamic multifactor hubs interact transiently with sites of active transcription in. *Elife* **7** (2018). https://doi.org/10.7554/eLife.40497

11 Du, M. *et al.* Direct observation of a condensate effect on super-enhancer controlled gene bursting. *Cell* **187**, 2595-2598 (2024). https://doi.org/10.1016/j.cell.2024.04.001

12 Guo, Y. E. *et al.* Pol II phosphorylation regulates a switch between transcriptional and splicing condensates. *Nature* **572**, 543-548 (2019). https://doi.org/10.1038/s41586-019-1464-0

13 Cho, W. K. *et al.* Mediator and RNA polymerase II clusters associate in transcription-dependent condensates. *Science* **361**, 412-415 (2018). https://doi.org/10.1126/science.aar4199

14 Forget, A. & Chartrand, P. Cotranscriptional assembly of mRNP complexes that determine the cytoplasmic fate of mRNA. *Transcription* **2**, 86-90 (2011). https://doi.org/10.4161/trns.2.2.14857

15 Viphakone, N. *et al.* Co-transcriptional Loading of RNA Export Factors Shapes the Human Transcriptome. *Mol Cell* **75**, 310-323.e318 (2019). https://doi.org/10.1016/j.molcel.2019.04.034

16 Garland, W. & Jensen, T. H. Nuclear sorting of RNA. *Wiley Interdiscip Rev RNA* **11**, e1572 (2020). https://doi.org/10.1002/wrna.1572

17 Percipalle, P. New insights into co-transcriptional sorting of mRNA for cytoplasmic transport during development. *Semin Cell Dev Biol* **32**, 55-62 (2014). https://doi.org/10.1016/j.semcdb.2014.03.009

18 Wende, W., Friedhoff, P. & Sträßer, K. Mechanism and Regulation of Co-transcriptional mRNP Assembly and Nuclear mRNA Export. *Adv Exp Med Biol* **1203**, 1-31 (2019). https://doi.org/10.1007/978-3-030-31434-7_1

19 Gehring, N. H., Wahle, E. & Fischer, U. Deciphering the mRNP Code: RNA-Bound Determinants of Post-Transcriptional Gene Regulation. *Trends Biochem Sci* **42**, 369-382 (2017). https://doi.org/10.1016/j.tibs.2017.02.004

20 Shahbabian, K. & Chartrand, P. Control of cytoplasmic mRNA localization. *Cell Mol Life Sci* **69**, 535-552 (2012). https://doi.org/10.1007/s00018-011-0814-3

21 Oleynikov, Y. & Singer, R. H. Real-time visualization of ZBP1 association with beta-actin mRNA during transcription and localization. *Curr Biol* **13**, 199-207 (2003). https://doi.org/10.1016/s0960-9822(03)00044-7

22 Butsch, M. & Boris-Lawrie, K. Destiny of unspliced retroviral RNA: ribosome and/or virion? *J Virol* **76**, 3089-3094 (2002). https://doi.org/10.1128/jvi.76.7.3089-3094.2002

23 Kaddis Maldonado, R. *et al.* The Rous sarcoma virus Gag Polyprotein Forms Biomolecular Condensates Driven by Intrinsically-disordered Regions. *J Mol Biol* **435**, 168182 (2023). https://doi.org/10.1016/j.jmb.2023.168182

24 Maldonado, R. J. K. *et al.* Visualizing Association of the Retroviral Gag Protein with Unspliced Viral RNA in the Nucleus. *mBio* **11** (2020). https://doi.org/10.1128/mBio.00524-20

25 Tuffy, K. M. *et al.* HIV-1 Gag Forms Ribonucleoprotein Complexes with Unspliced Viral RNA at Transcription Sites. *Viruses* **12** (2020). https://doi.org/10.3390/v12111281

26 Lochmann, T. L. *et al.* NC-mediated nucleolar localization of retroviral gag proteins. *Virus Res* **171**, 304-318 (2013). https://doi.org/10.1016/j.virusres.2012.09.011

27 Beyer, A. R. *et al.* Nucleolar trafficking of the mouse mammary tumor virus gag protein induced by interaction with ribosomal protein L9. *J Virol* **87**, 1069-1082 (2013). https://doi.org/10.1128/JVI.02463-12

28 Parent, L. J. New insights into the nuclear localization of retroviral Gag proteins. *Nucleus* **2**, 92-97 (2011). https://doi.org/10.4161/nucl.2.2.15018

29 Gudleski, N., Flanagan, J. M., Ryan, E. P., Bewley, M. C. & Parent, L. J. Directionality of nucleocytoplasmic transport of the retroviral gag protein depends on sequential binding of karyopherins and viral RNA. *Proc Natl Acad Sci U S A* **107**, 9358-9363 (2010). https://doi.org/10.1073/pnas.1000304107

30 Garbitt-Hirst, R., Kenney, S. P. & Parent, L. J. Genetic evidence for a connection between Rous sarcoma virus gag nuclear trafficking and genomic RNA packaging. *J Virol* **83**, 6790-6797 (2009). https://doi.org/10.1128/JVI.00101-09

31 Kenney, S. P., Lochmann, T. L., Schmid, C. L. & Parent, L. J. Intermolecular interactions between retroviral Gag proteins in the nucleus. *J Virol* **82**, 683-691 (2008). https://doi.org/10.1128/JVI.02049-07

32 Scheifele, L. Z., Kenney, S. P., Cairns, T. M., Craven, R. C. & Parent, L. J. Overlapping roles of the Rous sarcoma virus Gag p10 domain in nuclear export and virion core morphology. *J Virol* **81**, 10718-10728 (2007). https://doi.org/10.1128/JVI.01061-07

33 Butterfield-Gerson, K. L., Scheifele, L. Z., Ryan, E. P., Hopper, A. K. & Parent, L. J. Importin-beta family members mediate alpharetrovirus gag nuclear entry via interactions with matrix and nucleocapsid. *J Virol* **80**, 1798-1806 (2006). https://doi.org/10.1128/JVI.80.4.1798-1806.2006

34 Scheifele, L. Z., Ryan, E. P. & Parent, L. J. Detailed mapping of the nuclear export signal in the Rous sarcoma virus Gag protein. *J Virol* **79**, 8732-8741 (2005). https://doi.org/10.1128/JVI.79.14.8732-8741.2005

35 Chang, J. & Parent, L. J. HIV-1 Gag co-localizes with euchromatin histone marks at the nuclear periphery. *J Virol* **97**, e0117923 (2023). https://doi.org/10.1128/jvi.01179-23

36 Mullers, E., Stirnnagel, K., Kaulfuss, S. & Lindemann, D. Prototype foamy virus gag nuclear localization: a novel pathway among retroviruses. *J Virol* **85**, 9276-9285 (2011). https://doi.org/10.1128/JVI.00663-11

37 Rice, B. L., Kaddis, R. J., Stake, M. S., Lochmann, T. L. & Parent, L. J. Interplay between the alpharetroviral Gag protein and SR proteins SF2 and SC35 in the nucleus. *Front Microbiol* **6**, 925 (2015). https://doi.org/10.3389/fmicb.2015.00925

38 Kemler, I., Saenz, D. & Poeschla, E. Feline immunodeficiency virus Gag is a nuclear shuttling protein. *J Virol* **86**, 8402-8411 (2012). https://doi.org/10.1128/JVI.00692-12

39 Kemler, I., Meehan, A. & Poeschla, E. M. Live-cell coimaging of the genomic RNAs and Gag proteins of two lentiviruses. *J Virol* **84**, 6352-6366 (2010). https://doi.org/10.1128/JVI.00363-10

40 Monette, A. *et al.* Influence of HIV-1 Genomic RNA on the Formation of Gag Biomolecular Condensates. *J Mol Biol* **435**, 168190 (2023). https://doi.org/10.1016/j.jmb.2023.168190

41 Monette, A., Niu, M., Nijhoff Asser, M., Gorelick, R. J. & Mouland, A. J. Scaffolding viral protein NC nucleates phase separation of the HIV-1 biomolecular condensate. *Cell Rep* **40**, 111251 (2022). https://doi.org/10.1016/j.celrep.2022.111251

42 Monette, A. *et al.* Pan-retroviral Nucleocapsid-Mediated Phase Separation Regulates Genomic RNA Positioning and Trafficking. *Cell Rep* **31**, 107520 (2020). https://doi.org/10.1016/j.celrep.2020.03.084

43 Tunnacliffe, E. & Chubb, J. R. What Is a Transcriptional Burst? *Trends Genet* **36**, 288-297 (2020). https://doi.org/10.1016/j.tig.2020.01.003

44 Bertrand, E. *et al.* Localization of ASH1 mRNA particles in living yeast. *Mol Cell* **2**, 437-445 (1998).

45 Yang, J. H. & Hansen, A. S. Enhancer selectivity in space and time: from enhancer-promoter interactions to promoter activation. *Nat Rev Mol Cell Biol* **25**, 574-591 (2024). https://doi.org/10.1038/s41580-024-00710-6

46 Buchwalter, A., Kaneshiro, J. M. & Hetzer, M. W. Coaching from the sidelines: the nuclear periphery in genome regulation. *Nat Rev Genet* **20**, 39-50 (2019). https://doi.org/10.1038/s41576-018-0063-5

47 Scheifele, L. Z., Garbitt, R. A., Rhoads, J. D. & Parent, L. J. Nuclear entry and CRM1-dependent nuclear export of the Rous sarcoma virus Gag polyprotein. *Proc Natl Acad Sci U S A* **99**, 3944-3949 (2002). https://doi.org/10.1073/pnas.062652199

48 Marini, B. *et al.* Nuclear architecture dictates HIV-1 integration site selection. *Nature* **521**, 227-231 (2015). https://doi.org/10.1038/nature14226

49 Lambert, G. S., Rice, B. L., Maldonado, R. J. K., Chang, J. & Parent, L. J. Comparative analysis of retroviral Gag-host cell interactions: focus on the nuclear interactome. *Retrovirology* **21**, 13 (2024). https://doi.org/10.1186/s12977-024-00645-y

50 Mondal, A. & Kolomeisky, A. B. How Transcription Factors Binding Stimulates Transcriptional Bursting. *J Phys Chem Lett* **15**, 8781-8789 (2024). https://doi.org/10.1021/acs.jpclett.4c02050

51 Leyes Porello, E. A., Trudeau, R. T. & Lim, B. Transcriptional bursting: stochasticity in deterministic development. *Development* **150** (2023). https://doi.org/10.1242/dev.201546

52 Cisse, I. I. *et al.* Real-time dynamics of RNA polymerase II clustering in live human cells. *Science* **341**, 664-667 (2013). https://doi.org/10.1126/science.1239053

53 Cho, W. K. *et al.* Super-resolution imaging of fluorescently labeled, endogenous RNA Polymerase II in living cells with CRISPR/Cas9-mediated gene editing. *Sci Rep* **6**, 35949 (2016). https://doi.org/10.1038/srep35949
54 Ma, L. *et al.* Co-condensation between transcription factor and coactivator p300 modulates transcriptional bursting kinetics. *Mol Cell* **81**, 1682-1697.e1687 (2021). https://doi.org/10.1016/j.molcel.2021.01.031
55 Kane, M. *et al.* Nuclear pore heterogeneity influences HIV-1 infection and the antiviral activity of MX2. *Elife* **7** (2018). https://doi.org/10.7554/eLife.35738
56 D'Angelo, M. A. Nuclear pore complexes as hubs for gene regulation. *Nucleus* **9**, 142-148 (2018). https://doi.org/10.1080/19491034.2017.1395542
57 Maass, P. G., Barutcu, A. R. & Rinn, J. L. Interchromosomal interactions: A genomic love story of kissing chromosomes. *J Cell Biol* **218**, 27-38 (2019). https://doi.org/10.1083/jcb.201806052
58 Fanucchi, S., Shibayama, Y. & Mhlanga, M. M. Are genes switched on when they kiss? *Nucleus* **5**, 103-112 (2014). https://doi.org/10.4161/nucl.28352
59 Sabari, B. R., Dall'Agnese, A. & Young, R. A. Biomolecular Condensates in the Nucleus. *Trends Biochem Sci* **45**, 961-977 (2020). https://doi.org/10.1016/j.tibs.2020.06.007
60 Parent, L. J. *et al.* Positionally independent and exchangeable late budding functions of the Rous sarcoma virus and human immunodeficiency virus Gag proteins. *J Virol* **69**, 5455-5460 (1995).
61 Parent, L. J. *et al.* RNA dimerization defect in a Rous sarcoma virus matrix mutant. *J Virol* **74**, 164-172 (2000).
62 Moscovici, C. *et al.* Continuous tissue culture cell lines derived from chemically induced tumors of Japanese quail. *Cell* **11**, 95-103 (1977).
63 Gibson, D. G. *et al.* Enzymatic assembly of DNA molecules up to several hundred kilobases. *Nat Methods* **6**, 343-345 (2009). https://doi.org/10.1038/nmeth.1318
64 Crabbe, L., Cesare, A. J., Kasuboski, J. M., Fitzpatrick, J. A. & Karlseder, J. Human telomeres are tethered to the nuclear envelope during postmitotic nuclear assembly. *Cell Rep* **2**, 1521-1529 (2012). https://doi.org/10.1016/j.celrep.2012.11.019
65 Fusco, D. *et al.* Single mRNA molecules demonstrate probabilistic movement in living mammalian cells. *Curr Biol* **13**, 161-167 (2003).
66 Fusco, D., Bertrand, E. & Singer, R. H. Imaging of single mRNAs in the cytoplasm of living cells. *Prog Mol Subcell Biol* **35**, 135-150 (2004).
67 Li, L. *et al.* Real-time imaging of Huntingtin aggregates diverting target search and gene transcription. *Elife* **5** (2016). https://doi.org/10.7554/eLife.17056
68 Grimm, J. B. *et al.* A general method to improve fluorophores for live-cell and single-molecule microscopy. *Nat Methods* **12**, 244-250, 243 p following 250 (2015). https://doi.org/10.1038/nmeth.3256

Acknowledgements

Luke Lavis (HHMI Janelia Research Campus) kindly provided the SNAPTag JF549 and JF646 ligands. We thank Gregory S. Lambert, Alexis Davison, Padmani Rai, Alecia M. Achimovich, and Jordan Chang (Penn State College of Medicine) for critical discussions. We also thank Malgorzata Sudol for technical assistance. This work was supported by a grant from the National Institutes of Health, R01 GM139392 (L.J.P.).

Microscopy images and were generated and processed in the Penn State College of Medicine Advanced Light Microscopy Core (RRID: SCR_022526). The Advanced Light Microscopy Core services and instruments used in this project were funded, in part, by the Pennsylvania State University College of Medicine via the Office of the Vice Dean of Research and Graduate Students

and the Pennsylvania Department of Health using Tobacco Settlement Funds (CURE). The content is solely the responsibility of the authors and does not necessarily represent the views of the University or College of Medicine. The Pennsylvania Department of Health specifically disclaims responsibility for any analyses, interpretations or conclusions.

Author Contributions:

Conceptualization: R.J.K.M. and L.J.P.; Methodology: R.J.K.M. and L.J.P.; Formal analysis: R.J.K.M.; Investigation: R.J.K.M.; Resources: L.J.P.; Data Curation: R.J.K.M. and L.J.P.; Writing - Original Draft: R.J.K.M. and L.J.P.; Writing - Review & Editing: R.J.K.M. and L.J.P.; Visualization: R.J.K.M. and L.J.P.; Supervision: L.J.P.; Project administration: L.J.P.; Funding acquisition: L.J.P.

Conflicts of Interest:

Neither author declares conflicts of interest.

Correspondence and request for materials:

Correspondence can be addressed to either Rebecca J. Kaddis Maldonado: rjk297@psu.edu or Leslie J. Parent: lparent@psu.edu. Request for materials can be address to Leslie J. Parent: lparent@psu.edu.

A. QT6 rMACTIVE RC v8 MS2 stbl

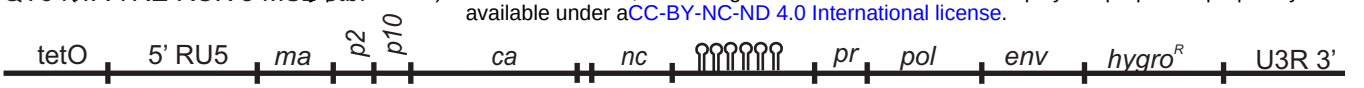

B. Still images extrancted from Supplementary Movie 1

Gag-SNAPTagJF549 + USvRNA (NES1-YFP-MS2-NLS)

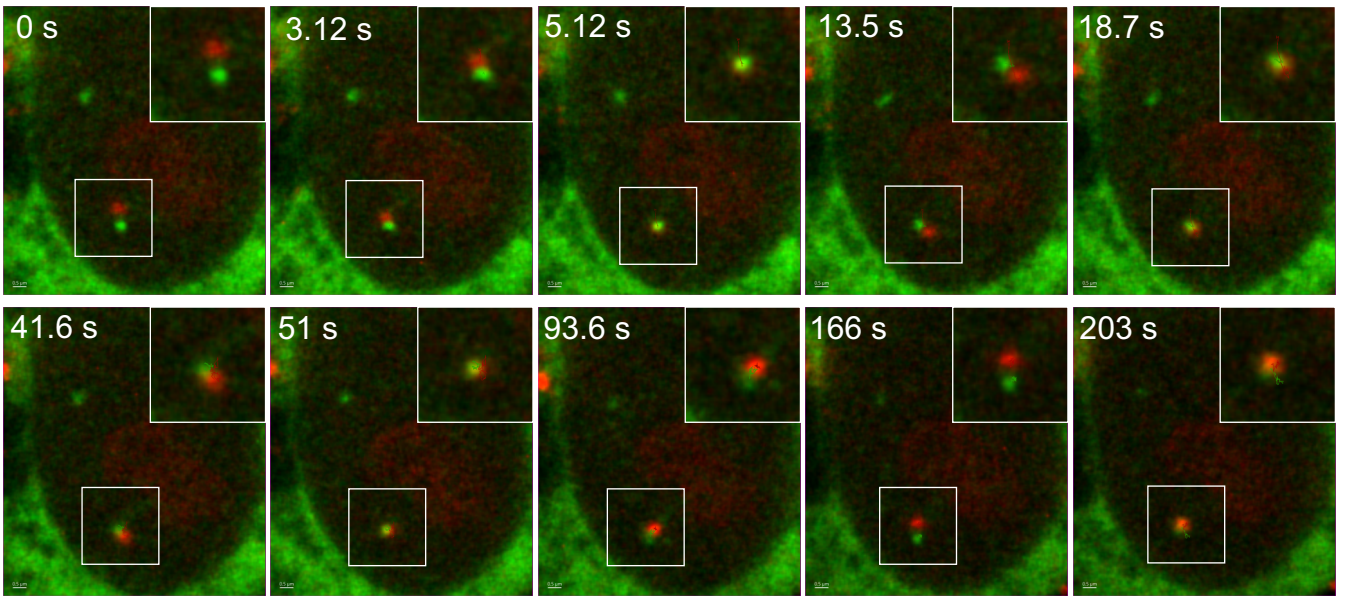

C. Distance between Gag condensate and USvRNA burst

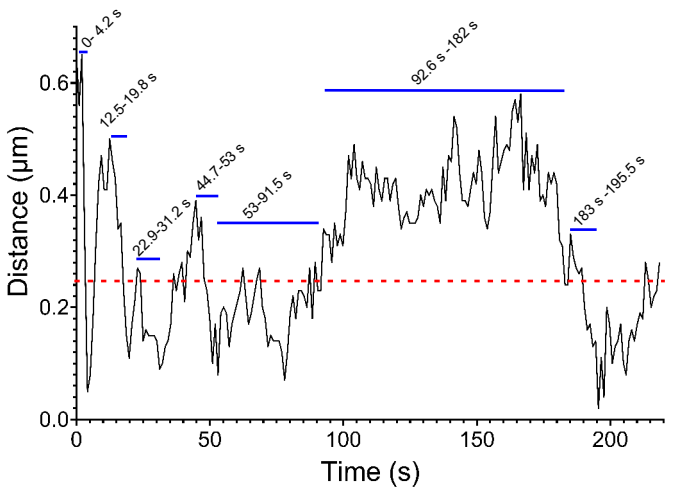

D. Intensities of Gag condensate and USvRNA burst

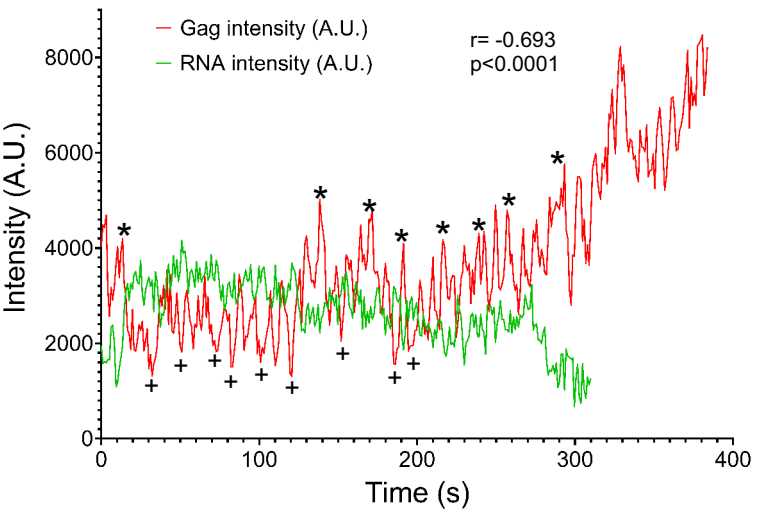

E. Gag and RNA areas over time

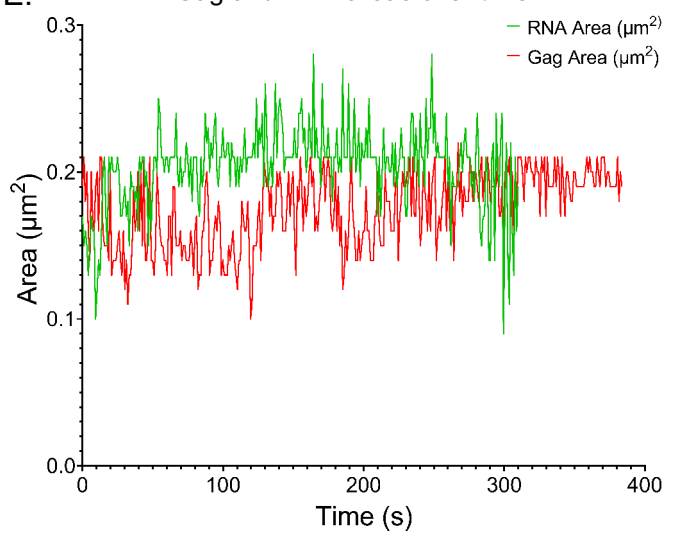

Figure 1

A. Still images extracted from Supplementary Movie 2

Gag-SNAPTagJF549 + USvRNA (NES1-YFP-MS2-NLS)

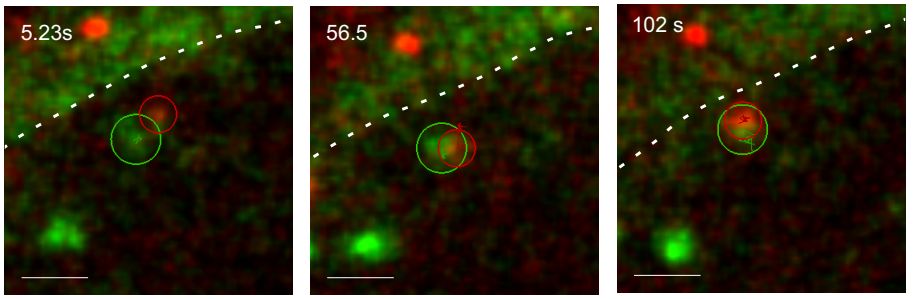

B. Distance between Gag condensate and USvRNA burst

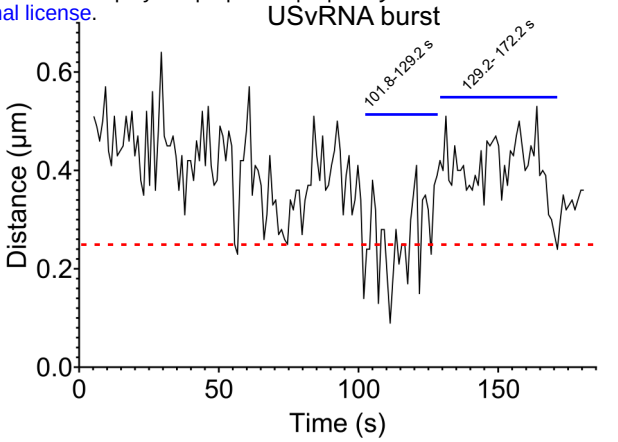

C. Intensities of Gag condensate and USvRNA burst

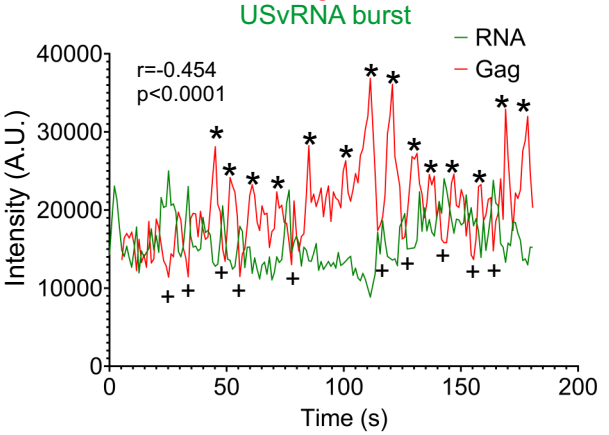

D. Still images extracted from Supplementary Movie 3

Gag-SNAPTagJF549 + USvRNA (NES1-YFP-MS2-NLS)

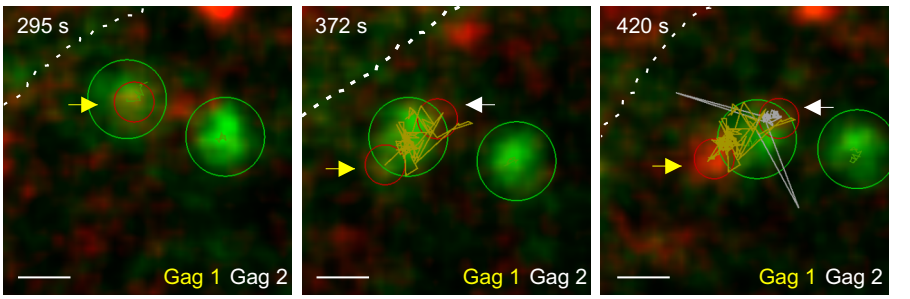

E. Distance between Gag condensate and USvRNA burst

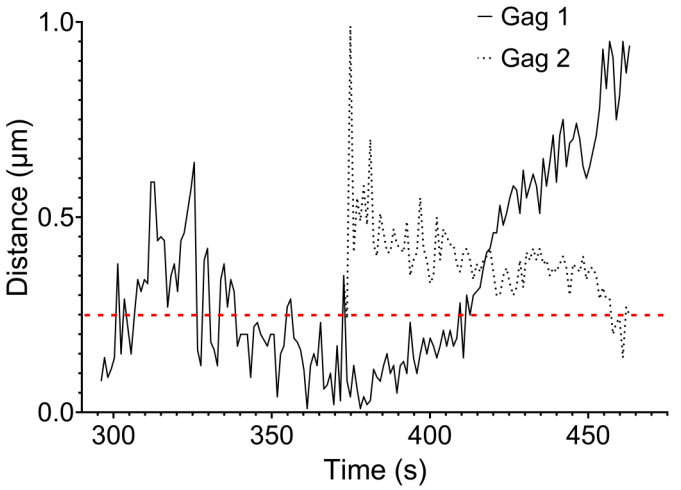

F. Intensities of Gag condensates and USvRNA burst

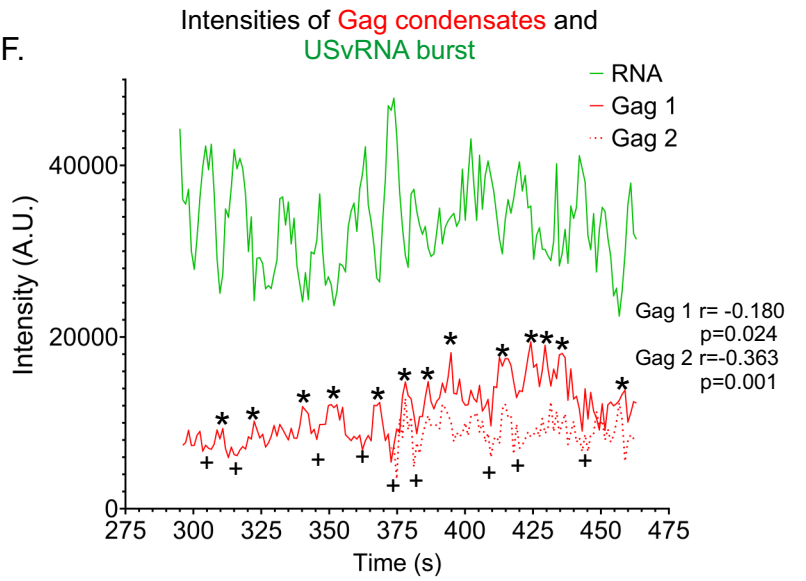

Figure 2

A. Still images extracted from Supplementary Movie 4

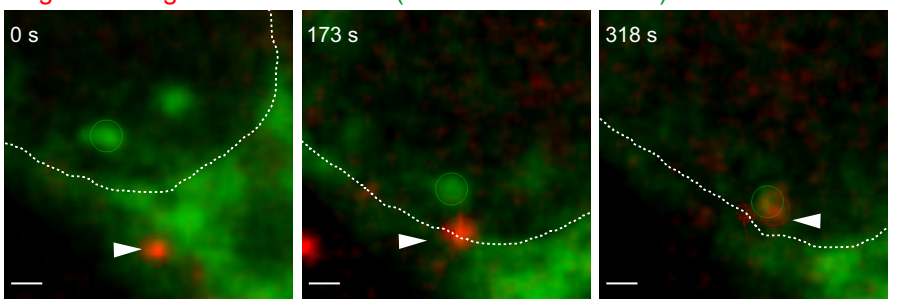

B. Distance between Gag condensate and USvRNA burst (Nucleus)

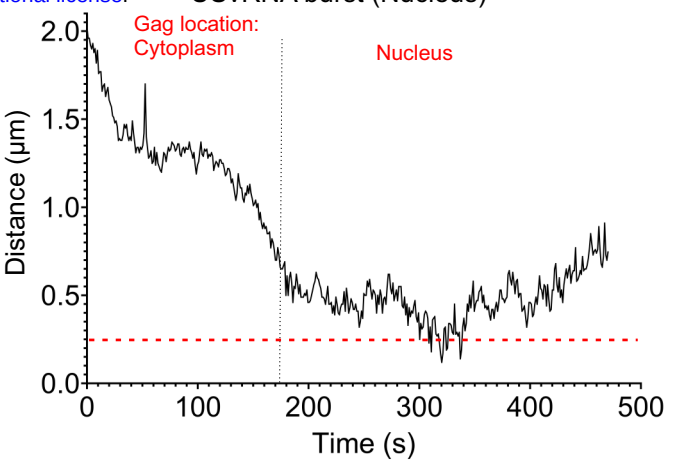

C. Intensities of Gag condensate and USvRNA burst

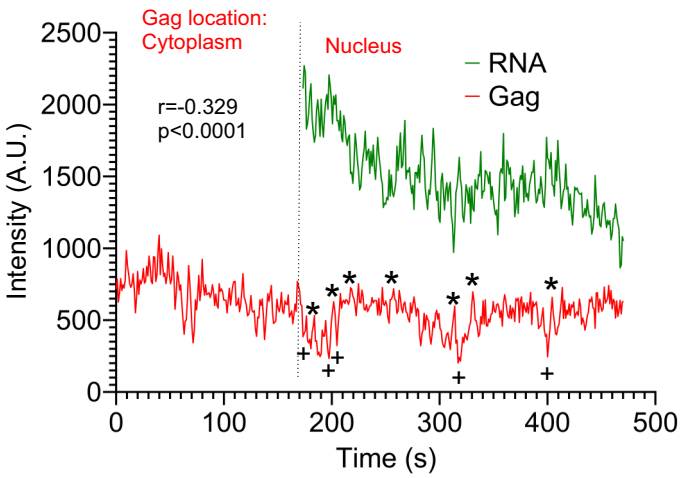

D. Still images extracted from Supplementary Movie 5

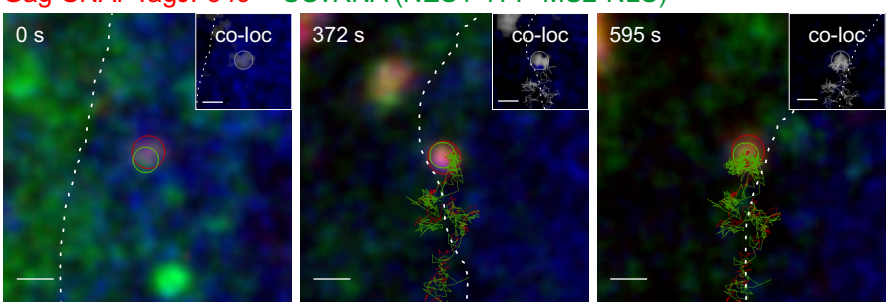

E. Distance between Gag condensate and USvRNA

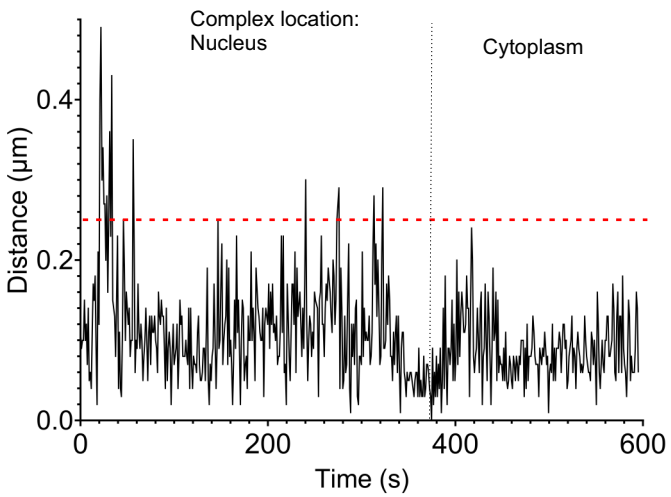

F. Intensity of Gag condensate and USvRNA

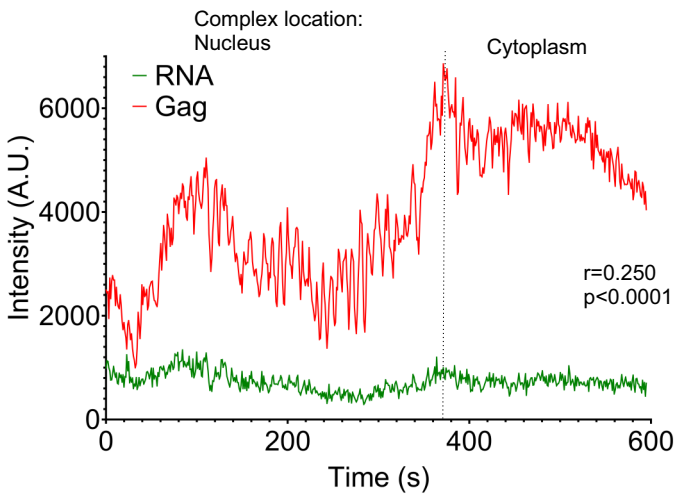

Figure 3

A. Still images extracted from Supplementary Movie 5

Gag-SNAPTagJF549 + USvRNA (NES1-YFP-MS2-NLS)

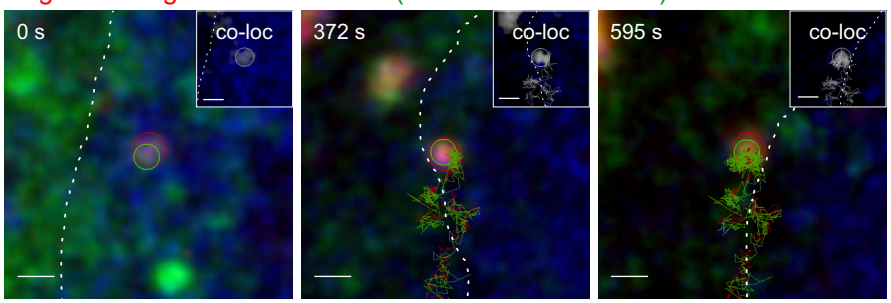

B. Distance between Gag condensate and USvRNA

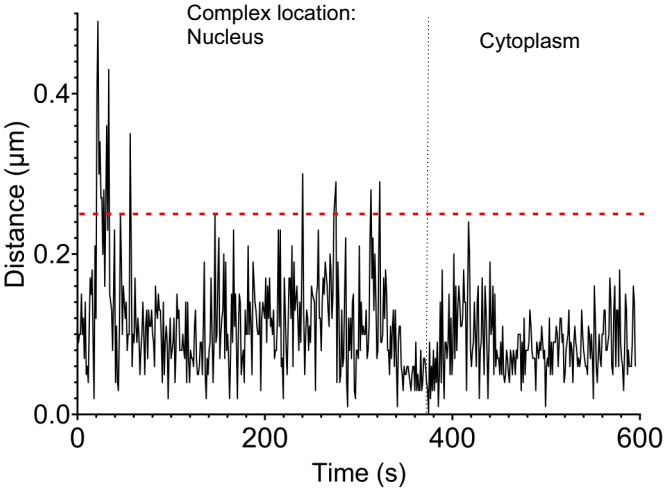

C. Intensity of Gag condensate and USvRNA

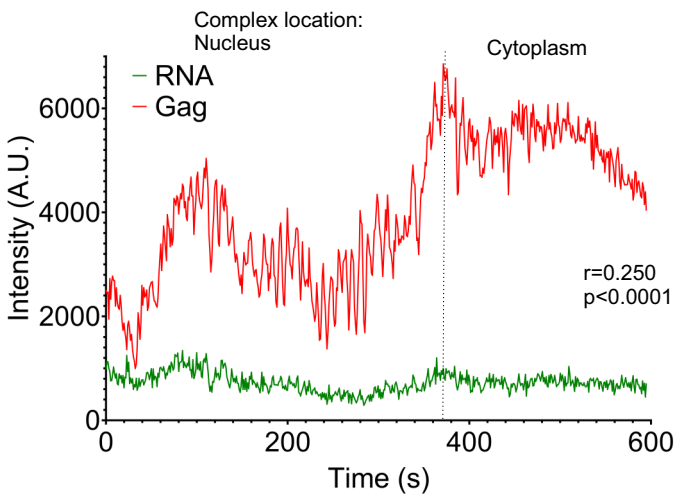

Figure 4

A. QT6 rMACTIVE RC.v8 Gag-SNAPTag M32 stbl

B.

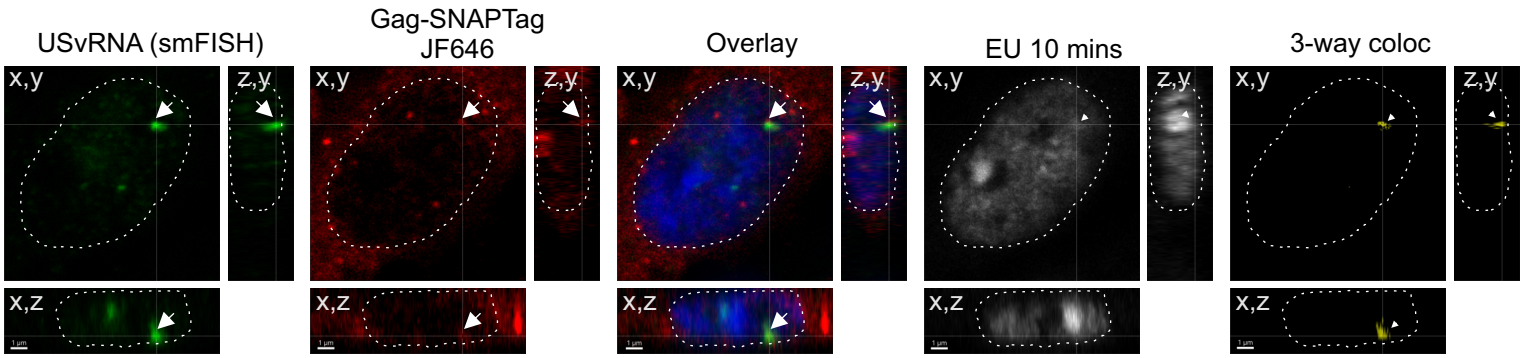

C. Enlarged images from panel B

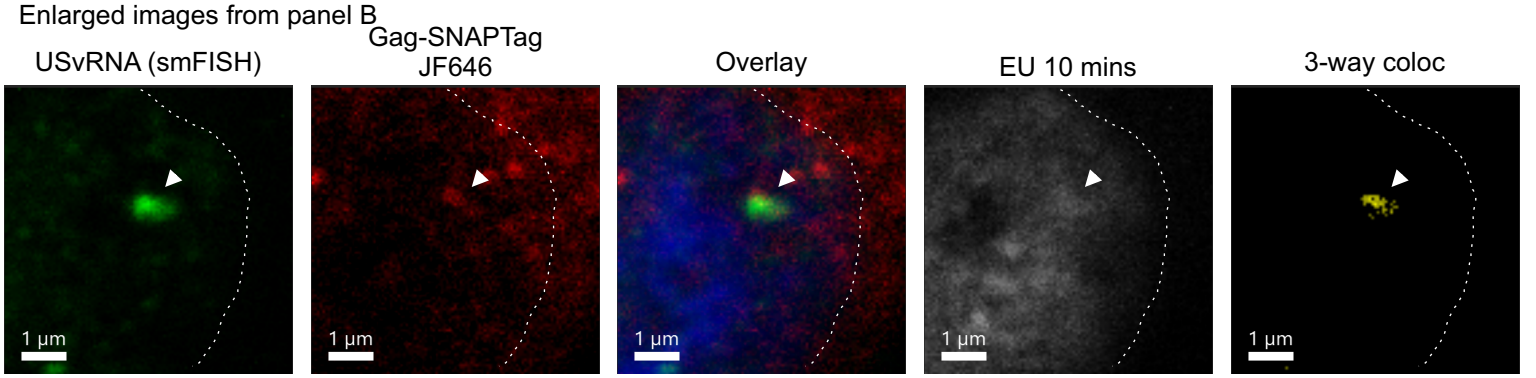

Figure 5

A.

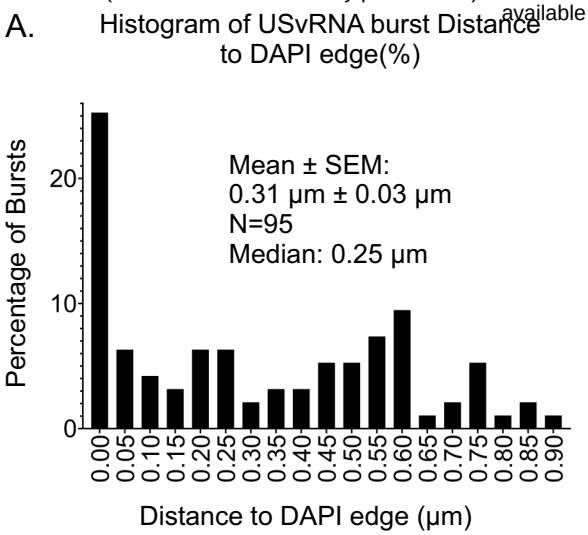

B.

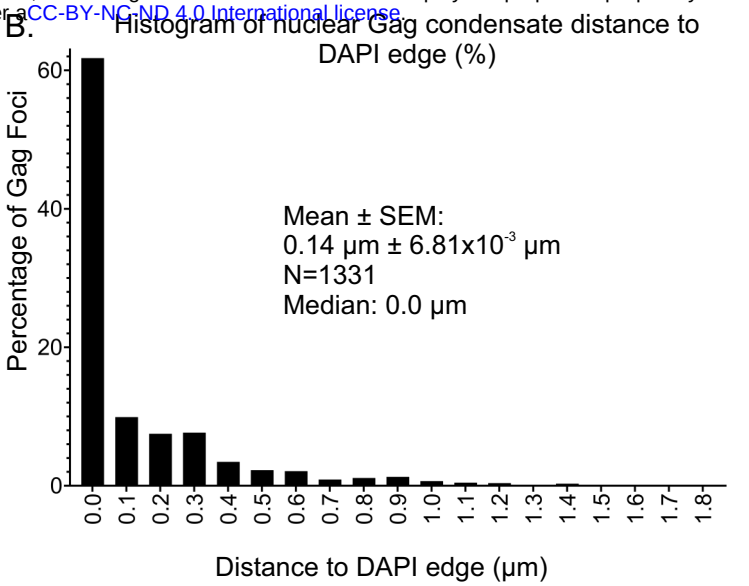

Figure 6

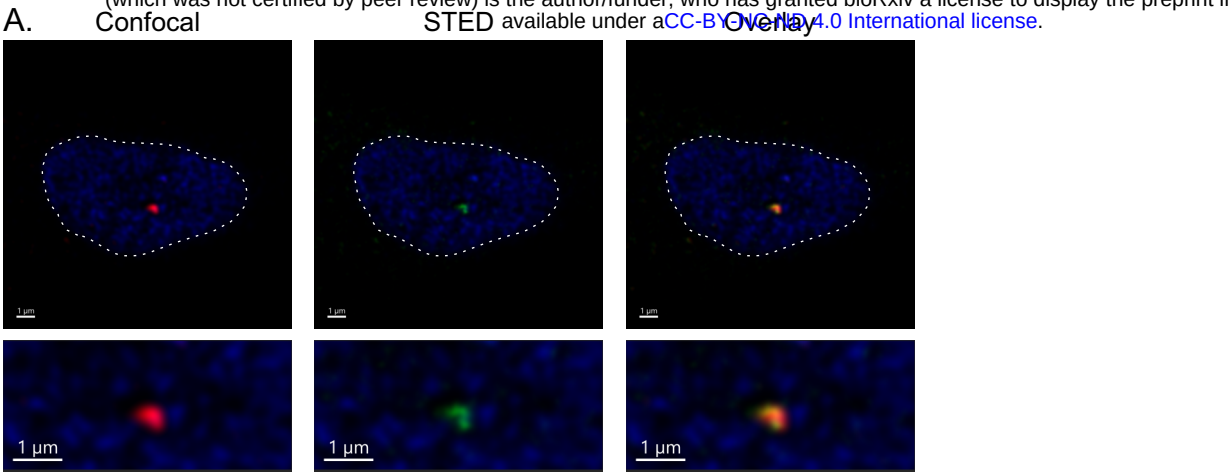

Figure 7

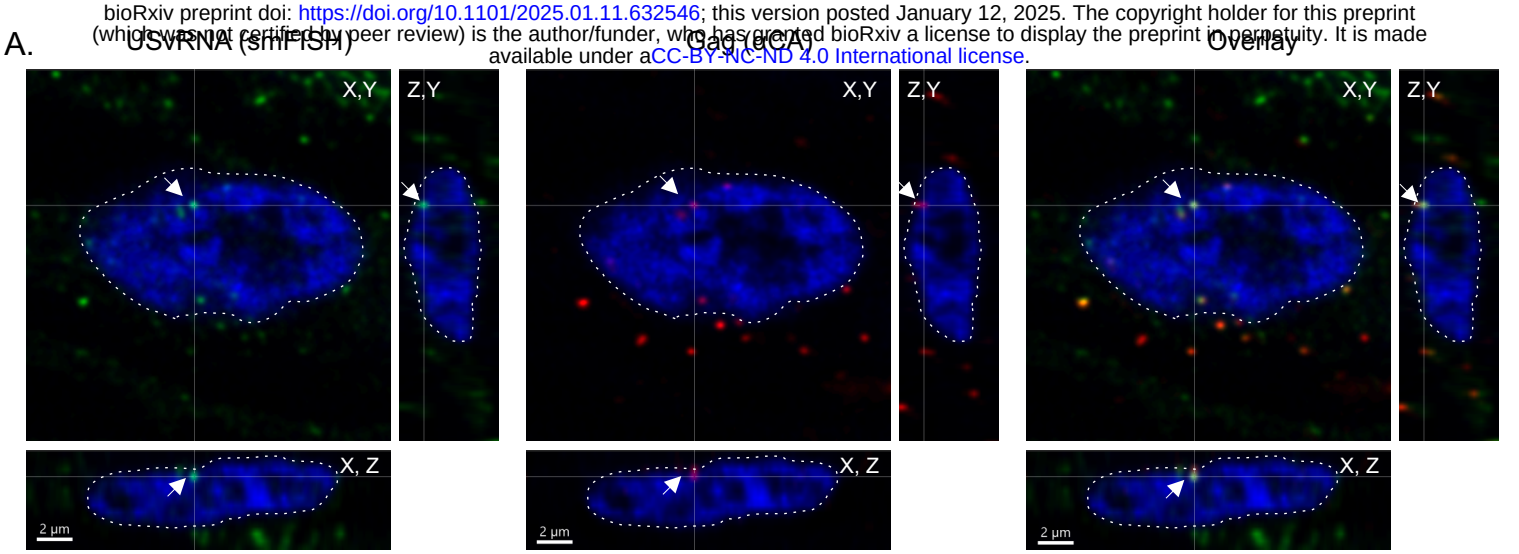

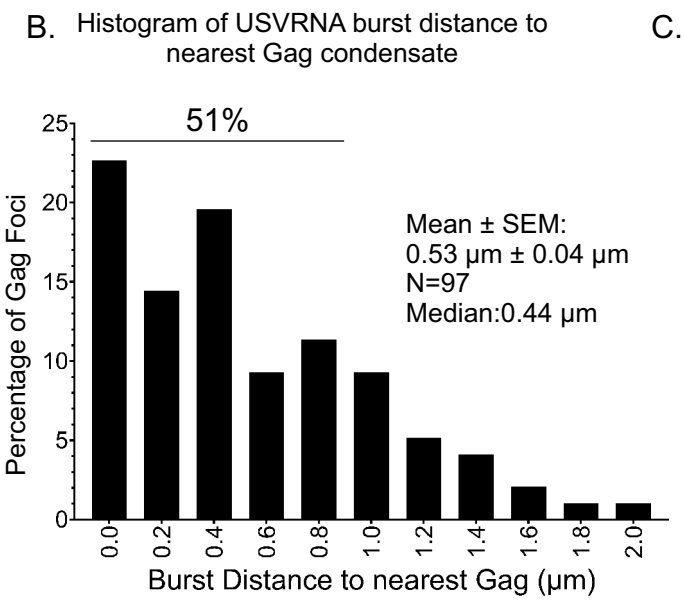

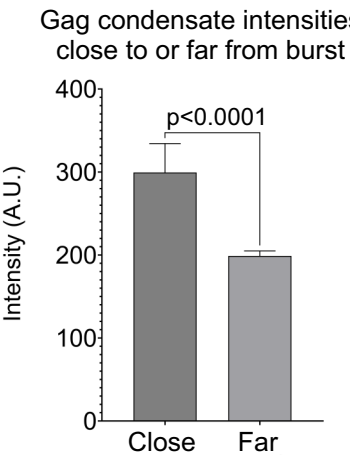

Close:
Mean ± SEM:
299.4 A.U. ±
34.96 A.U.
N=81
Median:160 A.U.

Far:
Mean ± SEM:
198.9 A.U. ±
6.14 A.U.
N=1024
Median:115.5 A.U.

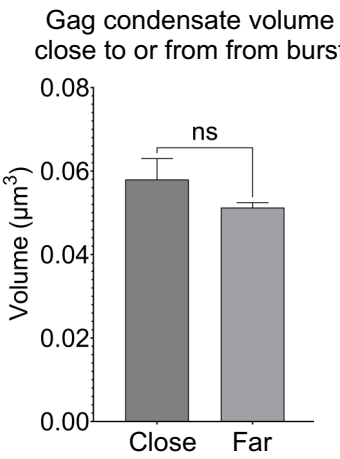

Close:
Mean ± SEM:
0.058 µm^3 ±
0.005 µm^3
N=90
Median:0.045

Far:
Mean ± SEM:
0.051 µm^3 ±
0.001 µm^3
N=1173
Median:0.040

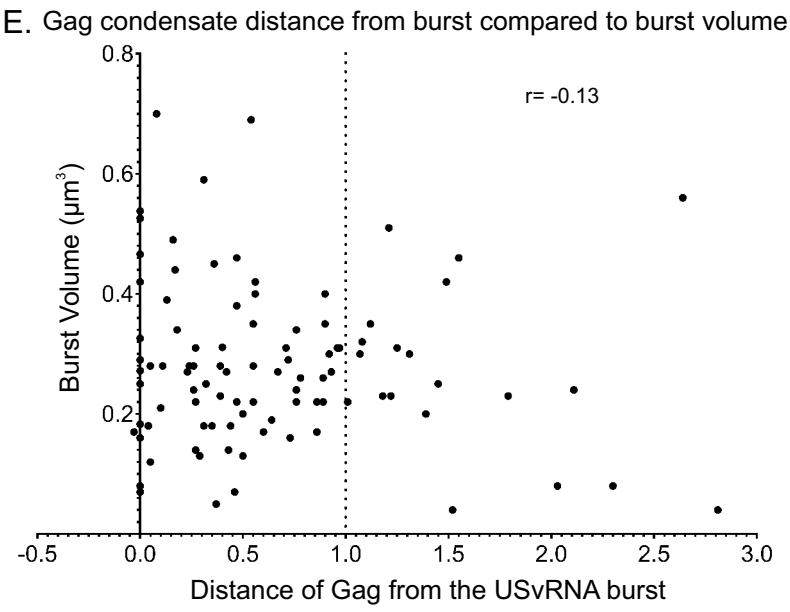

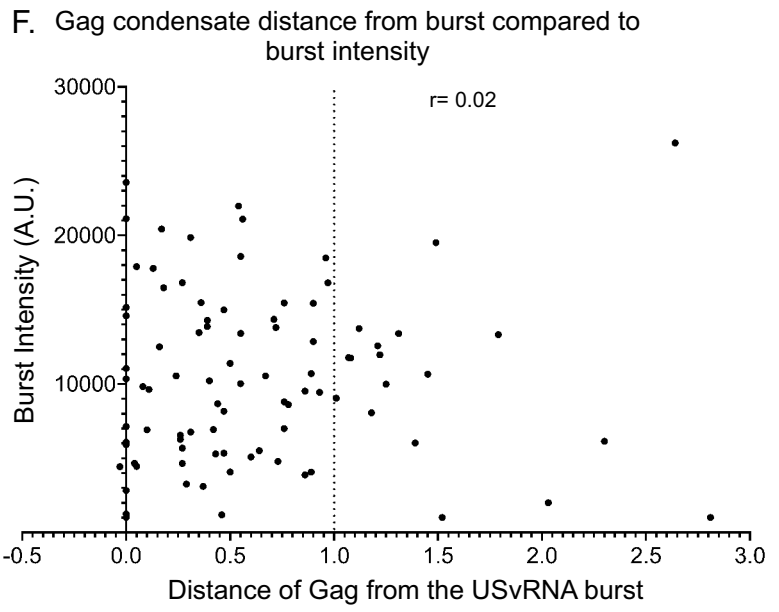

Figure 8

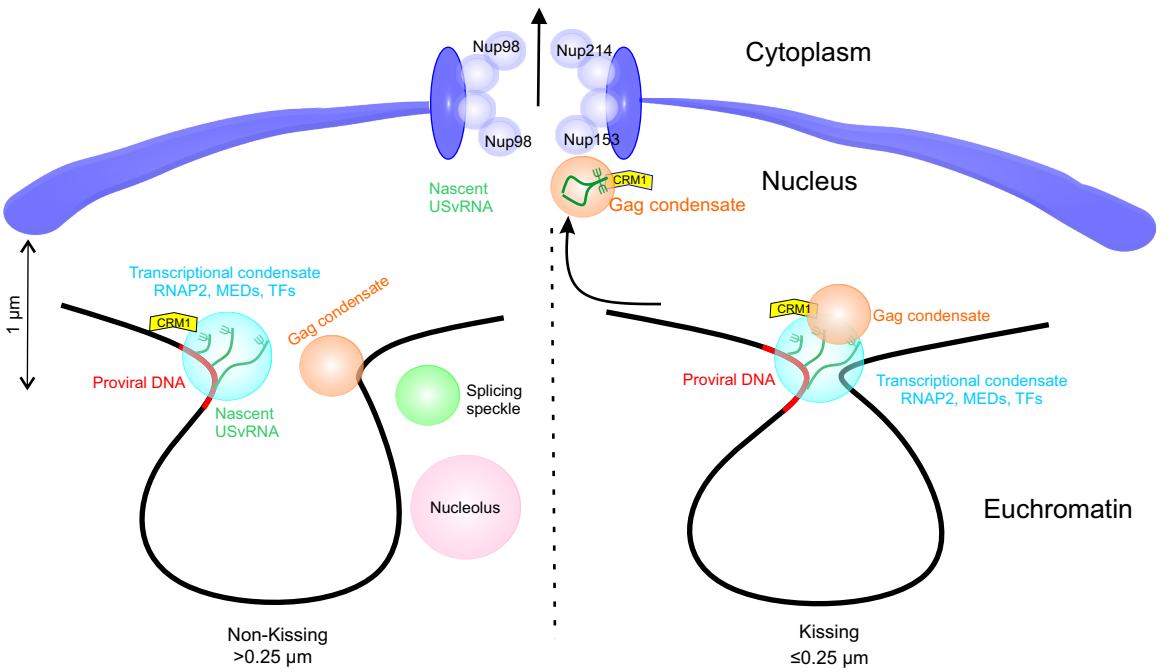

Figure 9

Figure 1: Live-cell time-lapse imaging of QT6 rtTA TRE RC.V8 MS2 stbl cell line. A) Schematic of the modified RSV provirus that was stably integrated into QT6 cells under control of a doxycycline-inducible promoter, and containing 24 copies of MS2 stable stemloops to label USvRNA. The QT6 rtTA TRE RC.V8 MS2 stbl cell line constitutively expresses rtTA. USvRNA was labeled by the MS2 coat protein fused to YFP, and containing an NLS and NES to enable MS2 to enter the nucleus while keeping nuclear background low (NES1-YFP-MS2-NLS).Cells were doxycycline-induced for ~22 hours and imaged every 1.04 s. **B)** Still images from Supplementary Movie 1 show multiple instances of Gag (red) and RNA "kissing." Examples of the foci "kissing" are shown. **C)** Peaks in the graph indicate the foci are apart while valleys correspond with foci within close proximity. Blue lines indicate the timepoints it takes for a peak to dip to a valley. **D)** The Gag and USvRNA are inversely correlated. r= -0.0693, p<0.0001. * indicates Gag peaks and + indicates Gag lows. **E)** The areas of Gag (red) and USvRNA (green) over the entire span of the movie.

Figure 2: Other instances of kissing between Gag and USvRNA observed via of live-cell time-lapse imaging of QT6 rtTA TRE RC.V8 MS2 stbl cell line. A) Stills correlating to Supplementary Movie 2. This cell was induced for ~16 hours and imaged every second. Scale bar = 1 µm. **B)** The distance between Gag and the burst remain within 1 µm. **C)** The Gag and USvRNA intensities are inversely correlated. R= -0.454, p<0.0001. Gag peaks are marked by * and lows are marked by +. **D)** Stills from Supplementary Movie 3 (16 hours post-induction, ~1 frame/second) showing multiple Gag condensates at two bursts. Gag 1 is marked with a yellow arrow and track. Gag 2 is marked by a white arrow and track. Scale bar = 0.5 µm. **E)** Both Gag condensates remained within 1 µm of the burst. **F)** The intensities of both Gag condensates are once again inversely correlated with that of the USvRNA burst. Gag 1: r= -0.180, p=0.024. Gag 2: r= -0.363, p=0.001. Gag peaks are marked by * and lows are marked by +. The nuclear rim is marked by the white dotted line.

Figure 3: Instance of Gag trafficking into the nucleus observed via live-cell time-lapse imaging of QT6 rtTA TRE RC.V8 MS2 stbl cell line. A) Stills correlating to Supplementary Movie 4 of a cell 2 hours post induction (imaged ~ 1 frame/ second) in which Gag (red) traffics from the cytoplasm into the nucleus (white outline) to the USvRNA burst (green) before undergoing kissing**.** Scale bar = 0.5 µm. **B)** The distance between Gag and USvRNA burst measured over time. The red text indicates the location of Gag during those time points and the dotted line indicates when Gag crosses into a new compartment. **C)** Intensities of Gag and USvRNA condensates overtime. USvRNA intensity is only being shown once Gag enters the nucleus. The Gag and USvRNA intensities are inversely correlated. r= -0.329, p<0.0001. Gag peaks are marked by * and lows are marked by +.

Figure 4: Instance of Gag-USvRNP trafficking out of the nucleus observed via live-cell time-lapse imaging of QT6 rtTA TRE RC.V8 MS2 stbl cell line. A) Stills correlating the Supplementary Movies 5 (overlay) and 6 (co-localization channel) showing a vRNP composed of Gag and USvRNA trafficking through the nucleus into the cytoplasm. **B)** The condensates remain within close proximity (<0.5 µm). **C)** The Gag and USvRNA intensities are positively correlated. r= 0.25, p<0.0001. The nuclear rim is marked by the white dotted line and/ or NucSpot650 (blue).

Figure 5: Gag co-localizes with nascent USvRNA at transcriptional bursts. A) QT6 rtTA TRE RC.V8 Gag-SNAPTag MS2 stbl cells constitutively express rtTA, and contain a stably integrated, modified RSV provirus that is under control of a doxycycline-inducible promoter, expresses a Gag-SNAPTag fusion protein, and contains 24 copies of MS2 stable stemloops to label USvRNA. **B)** QT6 rtTA TRE RC.V8 Gag-SNAPTag MS2 stbl cells were dox-induced for 48 hours. At 47 hpi, Gag-SNAPTag was labeled with SNAP ligand JF646 for 1 hour and in the last 10 minutes, cells were pulse labeled with EU. USvRNA was labeled via smFISH and EU labeled-RNAs were subjected to Click-chemistry to label them with Alexa 488. Z-stacks of cells were imaged via confocal microscopy and used to generate cross-sections. A burst of USvRNA (green), co-localized (white arrow) with Gag (red), and EU labeling (grey) in the nucleus (DAPI-blue, white outline). Three-way co-localization (yellow) was conducted to confirm this finding. Scale bar = 1 µm. **C)** An enlargement of the image presented in B. Scale bar = 1 µm.

Figure 6: USvRNA bursts and nuclear Gag localize near the nuclear rim. A) All bursts were within 1 µm of the nuclear rim (as marked by DAPI in three-dimensions), with an average of 0.31 µm ± 0.03 µm. **B)** 91.8% of Gag foci are present within 1 µm of the nuclear boundary, at an average distance of 0.14 µm ± 6.81×10^{-3} µm.

Figure 7: STED microscopy of USvRNA bursts reveals complex structures. A) Single z-slices of chronically infected cells comparing bursts of transcription imaged via confocal microscopy (red) to those imaged via STED (green). The nucleus is marked with Sun1-venus (blue, white outline). The image below is a zoom in of the burst of interest. The confocal burst appears as a single focus while the STED burst contains multiple smaller foci. Scale bar= 1 µm. **B)** Surface renderings were generated of the cell above and subjected to orthogonal clipping planes at either 0° or 90°. The STED bursts have a more lobed appearance. Scale bar= 1 µm. **C and D)** Two more examples of highly structured USvRNA bursts imaged via STED. The bursts are presented as a single Z-slice (Scale bar= 0.5 µm) or with an X,Y surface slicer (Scale bar=0.3-0.5 µm). In the bottom right corner of the bottom panels, a zoom in of a volume rendering of the bursts are presented (Scale bar= 0.07-0.1 µm). Both bursts appear lobed and highly structured.

Figure 8: Gag localizes in close proximity of transcriptional bursts in chronically infected cells. A) QT6 cells chronically infected with RSV with subjected to simultaneous smFISH to label USvRNA (green) and immunofluorescence to label Gag (red). Cells were imaged via confocal microscopy, and Z-stacks were used to generate cross-sections. A burst of USvRNA (green) co-localizes with Gag (red) in the nucleus (DAPI-blue, white outline). Scale bar = 2 µm. **B)** Histogram of USvRNA burst distance to nearest Gag focus. 51% of Gag nuclear foci are localized within 1 µm of the USvRNA burst with an average distance of 0.536 µm. (N=97 bursts). **C)** The average intensity of Gag nearest the burst (299.4 A.U. ± 34.96) was statistically significantly higher (****$p<0.0001$) than that of Gag foci away from the burst (198.9 A.U. ± 6.140 A.U.) while there was no significant difference in the volumes between Gag closest compared to those away from the burst **D)**. **E)** There is very low correlation between Gag distance from the burst and burst volume ($r = -0.13$) nor **F)** burst intensity ($r = 0.02$). Vertical dotted line indicates 1 µm distance from the burst.

Figure 9: Model for Gag interaction with USvRNA at transcriptional bursts. In the nucleus, Gag binds to a cellular factor such as mediator proteins, transcription factors, splicing factors, chromatin, or nucleoli. When the condensate “kisses” the RSV integrated provirus gene locus

where RNPII as part of the transcriptional condensate is transcribing USvRNA, Gag binds the USvRNA to form a viral ribonucleoprotein complex (vRNP). This complex is then exported from the nucleus through the nuclear pore via CRM1, traffics through the cytoplasm, and to the plasma membrane for virion assembly.

Supplementary Movie 1: The QT6 rtTA TRE RC.V8 MS2 stbl cell line that was transfected with Gag-SNAPTag JF549 (red) and NES1-YFP-MS2-NLS (USvRNA-green) and dox induced for approximately 22 hours. Cells were imaged every second. Particle tracking was conducted using the Imaris spot function. The USvRNA burst (green) and Gag focus (red) appear to be kissing in the nucleus. The nucleus is marked due to the NES1-YFP-MS2-NLS being able to clear the nucleus.

Supplementary Movie 2: The QT6 rtTA TRE RC.V8 MS2 stbl cell line was transfected with Gag-SNAPTag JF549 (red) and NES1-YFP-MS2-NLS (USvRNA-green) and dox induced for ~16 hours. Cells were imaged every second. Particle tracking was conducted using the Imaris spot function. One of the bursts burst of USvRNA (green) in the nucleus was met by a red focus of Gag to undergo a kissing interaction. The nucleus was marked based on the NES1-YFP-MS2-NLS signal.

Supplementary Movie 3: The QT6 rtTA TRE RC.V8 MS2 stbl cell line that was transfected with Gag-SNAPTag JF549 (red) and NES1-YFP-MS2-NLS (USvRNA-green) and dox induced for ~16 hours. Cells were imaged every second. Particle tracking was conducted using the Imaris spot function. Two Gag foci (red) were tracked to the same burst of USvRNA (green). Gag condensate 1: Yellow track. Gag condensate 2: White track. The nucleus is marked based on the NES1-YFP-MS2-NLS signal. This is the same cell imaged in Supplemental Movie 2 but at an earlier time point.

Supplementary Movie 4: The QT6 rtTA TRE RC.V8 MS2 stbl cell line that was transfected with Gag-SNAPTag JF549 (red) and NES1-YFP-MS2-NLS (USvRNA-green) and dox induced for 2 hours. Cells were imaged every second. Particle tracking was conducted using the Imaris spot function. A focus of Gag (red) was tracked from the cytoplasm into the nucleus and kissed the USvRNA burst (green). The nucleus is marked due to the NES1-YFP-MS2-NLS being able to clear the nucleus.

Supplementary Movie 5: The QT6 rtTA TRE RC.V8 MS2 stbl cell line was transfected with Gag-SNAPTag JF549 (red) and NES1-YFP-MS2-NLS (USvRNA-green) and dox induced for ~22 hours. Cells were imaged every second. Particle tracking was conducted using the Imaris spot function. A focus USvRNA (green), not correlating to a burst, in the nucleus formed a vRNP with Gag that trafficked from the nucleus into the cytoplasm. The nucleus was labeled with NucSpot 650.

Supplemental Movie 6: This channel shows the tracking of the co-localization channel generated from the USvRNA and Gag signals from the movie presented in 5.

Supplementary Table 1: Burst distance to DAPI Edge										
Bin Center Distance From DAPI edge (µm)	**0.00**	**0.1**	**0.2**	**0.3**	**0.4**	**0.5**	**0.6**	**0.7**	**0.8**	**0.9**
Number of Bursts	27	8	13	5	4	12	14	4	6	2

Supplementary Table 2: Gag distance to DAPI Edge																		
Bin Number Distance to DAPI Edge (µm)	**0.00**	**0.10**	**0.20**	**0.30**	**0.40**	**0.50**	**0.60**	**0.70**	**0.80**	**0.90**	**1.00**	**1.10**	**1.20**	**1.30**	**1.40**	**1.50**	**1.60**	**1.70**	**1.80**
Number of Gag foci	822	132	100	102	46	30	28	12	15	17	9	6	5	0	4	1	1	0	1

923